Cell Reports

Article

Endothelin-1 drives invadopodia and interaction with mesothelial cells through ILK

Graphical abstract

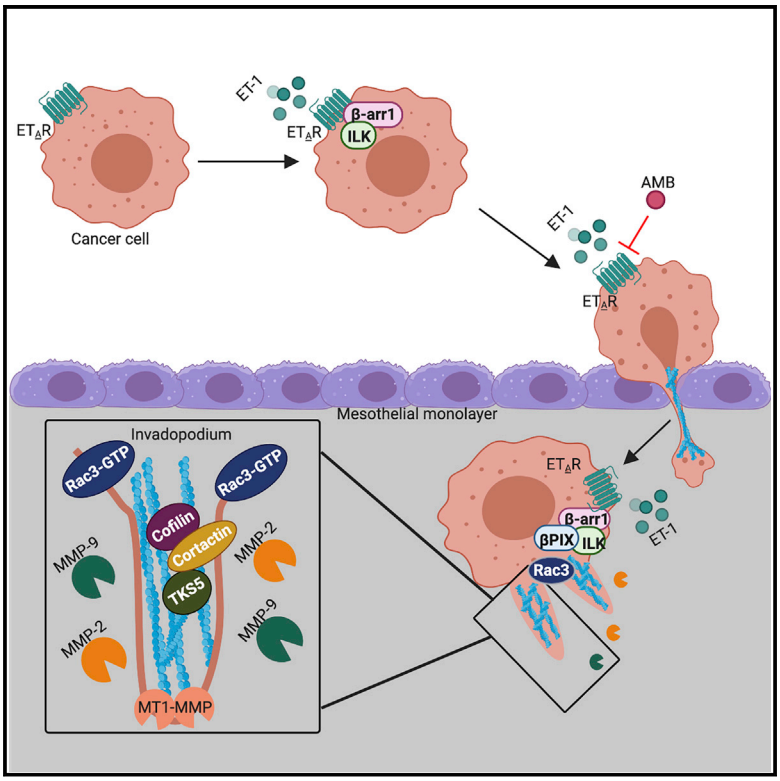

Highlights

- ET$_A$R/β-arr1 and ILK activate Rac3 GTPase, PAK1, and cofilin pathways through βPIX
- ET$_A$R/ILK/β-arr1/Rac3 regulates invadopodia, ECM proteolysis, and cell invasion
- ET$_A$R/β-arr1/ILK facilitates SOC/mesothelial cells interactions
- Ambrisentan inhibits *in vivo* adhesion and metastatic spread of SOC cells

Authors

Ilenia Masi, Valentina Caprara, Francesca Spadaro, ..., Alberto Rainer, Anna Bagnato, Laura Rosanò

Correspondence

laura.rosano@uniroma1.it

In brief

Unraveling mechanisms governing cancer spread are an unmet need in cancer therapeutics. Masi et al. uncover an integrin linked kinase as an interactor of endothelin A receptor/β-arr1 in the establishment of ovarian cancer-stroma interactions and in directing invadopodia-mediated invasion.

Masi et al., 2021, Cell Reports *34*, 108800
March 2, 2021 © 2021 The Author(s).
https://doi.org/10.1016/j.celrep.2021.108800

CellPress

Cell Reports

CellPress
OPEN ACCESS

Article

Endothelin-1 drives invadopodia and interaction with mesothelial cells through ILK

Ilenia Masi,[1,7] Valentina Caprara,[1,7] Francesca Spadaro,[2] Lidia Chellini,[1] Rosanna Sestito,[1] Andrea Zancla,[3,4] Alberto Rainer,[3,5] Anna Bagnato,[1] and Laura Rosanò[1,6,8,*]

[1]Unit of Preclinical Models and New Therapeutic Agents, IRCCS - Regina Elena National Cancer Institute, Rome 00128, Italy
[2]Confocal Microscopy Unit, Core Facilities, Istituto Superiore di Sanità, Rome 00161, Italy
[3]Department of Engineering, Università Campus Bio-Medico di Roma, via Álvaro del Portillo 21, Rome 00128, Italy
[4]Department of Engineering, Università degli Studi Roma Tre, via Vito Volterra 62, Rome 00146, Italy
[5]Institute of Nanotechnology (NANOTEC), National Research Council (CNR), c/o Campus Ecotekne, via Monteroni, Lecce 73100, Italy
[6]Institute of Molecular Biology and Pathology, National Research Council (CNR), Rome 00185, Italy
[7]These authors contributed equally
[8]Lead contact
*Correspondence: laura.rosano@uniroma1.it
https://doi.org/10.1016/j.celrep.2021.108800

SUMMARY

Cancer cells use actin-based membrane protrusions, invadopodia, to degrade stroma and invade. In serous ovarian cancer (SOC), the endothelin A receptor (ET_AR) drives invadopodia by a not fully explored coordinated function of β-arrestin1 (β-arr1). Here, we report that β-arr1 links the integrin-linked kinase (ILK)/βPIX complex to activate Rac3 GTPase, acting as a central node in the adhesion-based extracellular matrix (ECM) sensing and degradation. Downstream, Rac3 phosphorylates PAK1 and cofilin and promotes invadopodium-dependent ECM proteolysis and invasion. Furthermore, ET_AR/ILK/Rac3 signaling supports the communication between cancer and mesothelial cells, favoring SOC cell adhesion and transmigration. *In vivo*, ambrisentan, an ET_AR antagonist, inhibits the adhesion and spreading of tumor cells to intraperitoneal organs, and invadopodium marker expression. As prognostic factors, high *EDNRA/ILK* expression correlates with poor SOC clinical outcome. These findings provide a framework for the ET-1R/β-arr1 pathway as an integrator of ILK/Rac3-dependent adhesive and proteolytic signaling to invadopodia, favoring cancer/stroma interactions and metastatic behavior.

INTRODUCTION

Invadopodia are actin-rich membrane extensions used by cancer cells to degrade the extracellular matrix (ECM), a non-cellular structure comprising the basement membrane and the collagen-based interstitial matrix (Murphy and Courtneidge, 2011; Paterson and Courtneidge, 2018; Eddy et al., 2017). Their functional activity requires the coordination of complex molecular machinery, including the arrangement of an F-actin-cortactin core surrounded by actin regulatory proteins, such as ARP2/3, N-WASP, cofilin, and actin cross-linking proteins, the presence of scaffolding, adhesion, and signaling-associated proteins for the stabilization, and the continuous delivery of proteases, ensuring ECM proteolytic degradation and penetration by cancer cells (Eddy et al., 2017; Paterson and Courtneidge, 2018). Several growth factors, among other stimuli, might induce invadopodia, generating signaling cues implicated from the initial steps of anchoring and protein recruitment to the final steps of matrix degradation or structure disassembling (Masi et al., 2020). Integrins and associated proteins operate in the same subcellular compartments promoting the recruitment of matrix metalloproteinases (MMPs) especially the transmembrane MMP, MT1-MMP, which is essential for invadopodia-mediated pericellular matrix degradation and cell invasion (Badowski et al., 2008; Takkunen et al., 2010; Destaing et al., 2011; Branch et al., 2012; Antelmi et al., 2013; Beaty et al., 2013; Hoshino et al., 2013; Revach and Geiger, 2014; Parekh and Weaver, 2016; Peláez et al., 2017, 2019). In this context, integrins and the protein integrin-linked kinase (ILK) are needed for adhesion ring formation, localization of the vesicular adaptor protein IQ-domain GTPase-activating protein 1 (IQGAP1), and MT1-MMP to invadopodia, overall controlling invadopodium maturation and ECM degradation (Sakurai-Yageta et al., 2008; Petropoulos et al., 2016).

ILK is a well-known serine/threonine kinase and multidomain adaptor located in close association with integrin cytoplasmic tails, used by cancer cells to sense the surrounding and to transmit signals from the ECM to the actin cytoskeleton (McDonald et al., 2008; Cabodi et al., 2010). ILK regulates cytoskeletal reorganization by activating Rac1 and Cdc42 GTPases, critically involved in the invadopodia life cycle (McDonald et al., 2008). High expression of ILK is associated with high-grade human tumors and metastatic cancer cell phenotypes, including in serous ovarian cancer (SOC) (Ahmed et al., 2003; Graff et al., 2001; Engelman et al., 2013; Bruney et al., 2016). Although ILK can direct

This is an open access article under the CC BY license (http://creativecommons.org/licenses/by/4.0/).

invadopodium-associated ECM degradation, its functional regulation in the invadopodia life cycle is still not well known.

As a focal point for signaling pathways regulating cytoskeleton reorganization and cell motility, the growth factor endothelin-1 (ET-1) acting through the type A receptor (ET_AR), belonging to the large G-protein-coupled receptor (GPCR) family, is a driver of invadopodia (Rosanò et al., 2013a; Masi et al., 2020). Active ET_AR recruits the scaffold protein β-arrestins (β-arrs) and functional interactions of β-arr1 or β-arr2 with many signaling proteins in cytosolic or nuclear compartments strongly contribute to the tumor-promoting activities (Rosanò et al., 2009, 2013b; Smith and Rajagopal, 2016; Tocci et al., 2019). The β-arr functional divergence depends on their differential interactions with specific proteins or on the different subcellular localization (Peterson and Luttrell, 2017; Jean-Charles et al., 2017). The multitask β-arr isoforms, acting as a signal transducers of GPCR, facilitate an intricate signaling interchange that rules different cellular effects in malignant disease. An increasing body of evidence has demonstrated that, although SOC cells express both β-arrs (Rosanò et al., 2009), downstream of ET_AR, β-arr1 coordinates invadopodia formation and proteolytic activity (Rosanò and Bagnato, 2019). β-arr1 interactions determine the convergence and activation/inhibition of specific signals at invadopodia, as the Rho GTPases and their regulators (Rosanò and Bagnato, 2019). RhoC is the main Rho GTPase regulated by β-arr1 through the interaction with PDZ-RhoGEF and the actin regulator hMENA/hMENAΔv6. The activity and the spatial distribution of RhoC represents a critical route by which the tumor cells control the recruitments of cortactin, TKS5, and MMPs in the formation of non-degradative invadopodium precursors, and the spatial restriction of cofilin activity, starting the maturation process (Semprucci et al., 2016; Di Modugno et al., 2018; Purayil and Daaka, 2018), further highlighting the interaction network of β-arr proteins in controlling cytoskeleton dynamics (Masi et al., 2020; DeFea, 2013).

Considering that ILK can be regulated by ET-1 signaling (Rosanò et al., 2006), and that adhesion rings surrounding invadopodia promote targeted protease recruitment by a mechanism linking ILK and IQGAP1 (Branch et al., 2012), in this study, we addressed the role of ILK in ET-1/β-arr1 signaling and to what extent ILK could enhance invadopodium activity in SOC progression. Moreover, since the importance of the communication between cancer and stromal cells in supporting the invadopodium-mediated invasion, we evaluated also ET_AR/ILK-driven signaling in the interaction of SOC cells with mesothelial cells, further reinforcing their invasive behavior. Finally, we tested the utility of blocking ET_AR signaling in preventing invadopodium activity, tumor cell adhesion, and peritoneal spread in SOC xenografts.

RESULTS

High ILK/ET_AR expression is associated with poor prognosis in serous ovarian cancer patients

A previous study reported a positive correlation between high expression of ILK and high-grade SOC, compared to weak staining in low-grade lesions (Ahmed et al., 2003). Moreover, analysis of OC tissues demonstrated that ET_AR overexpression is associated with worse survival in advanced stages (Rosanò et al., 2014). Therefore, we investigated the prognostic significance of *EDNRA* (ET_AR) and *ILK* mRNA expression in SOC patients by using the TCGA dataset. Kaplan-Meier analysis and the log-rank test evaluating median expression values of combined *EDNRA* and *ILK* mRNAs demonstrated that the survival rate of SOC patients with high *EDNRA*/*ILK* expression, in terms of overall survival (OS) and progression-free survival (PFS), is significantly worse than those in low-expression groups (Figure 1A), supporting the use of ET_AR/ILK as potential prognostic biomarkers in SOC patients.

ILK/βPIX are new interactors of β-arr1 in ET-1-dependent manner

Emerging data established that ILK is a key effector of invadopodium stability and ILK is a key effector of invadopodium stability and maturation (Branch et al., 2012). In the GEF family, the p21-activated kinase (PAK)-interacting exchange factors PIXα/β are partners of ILK in controlling Rho GTPase activity (Bagrodia et al., 1998; Baird et al., 2005), and βPIX is implicated in invadopodia (Md Hashim et al., 2013; Ward et al., 2015; Donnelly et al., 2017). Since ET-1 might induce βPIX translocation to focal complexes (Chahdi et al., 2005) and βPIX might also mediate ET-1 signaling (Chahdi and Sorokin, 2006), we investigated whether ILK and βPIX might interact with β-arr1 to regulate invadopodia signaling downstream of ET_AR. In a panel of SOC cells, SKOV3, OVCAR3, and CAOV3, RT-PCR, and western blotting (WB) analyses demonstrated that ILK and βPIX (*PIXB*) are expressed in all cell lines, at the mRNA and protein level, along with β-arr1 (*ARRB1*) (Figures 1B and S1A). To uncover whether β-arr1 can interact with ILK or βPIX, we used different approaches. As shown by co-immunoprecipitation (co-IP) assays followed by WB analyses, ET-1 addition facilitates the interaction of β-arr1 with both βPIX and ILK, after 30 min of stimulation, while this effect is absent in the presence of the ET_AR antagonist ambrisentan but not of the ET_BR antagonist BQ788 (Figures 1C, 1D, S1B, and S1C). Similar results have been found upon silencing of ET_AR and rescue with an ET_AR-GFP plasmid (Figure S1D), confirming that ET_AR is the main receptor involved in this process. Since SOC cells also express β-arr2 (Figure S1E), we evaluated the interaction of β-arr2 with ILK and βPIX. ET-1 promotes the interaction of β-arr2 with βPIX but not with ILK (Figure S1F), leading us to focus only on the interaction of β-arr1. To further demonstrate the interaction of endogenous β-arr1 with ILK and βPIX, we used also *in situ* proximity ligation assay (PLA) technology to visualize the interaction between two proteins that are in close proximity. βPIX/β-arr1 and ILK/β-arr1-containing spots were significantly more numerous when ET-1 was added to cells, while this effect was impaired upon treatment with ambrisentan (Figure 1E and S2A). The interaction between βPIX or ILK and β-arr1 was also confirmed by using GST pull-down assays and β-arr1 fusion protein, demonstrating a direct interaction between endogenous βPIX or ILK and GST-β-arr1 fusion protein (Figure S2B). Of note, by using cells expressing AU5-β-arr1, the formation of a trimeric complex comprising β-arr1 with both βPIX and ILK was shown upon stimulation with ET-1 but not in the presence of ambrisentan (Figure S2C).

CellPress
OPEN ACCESS

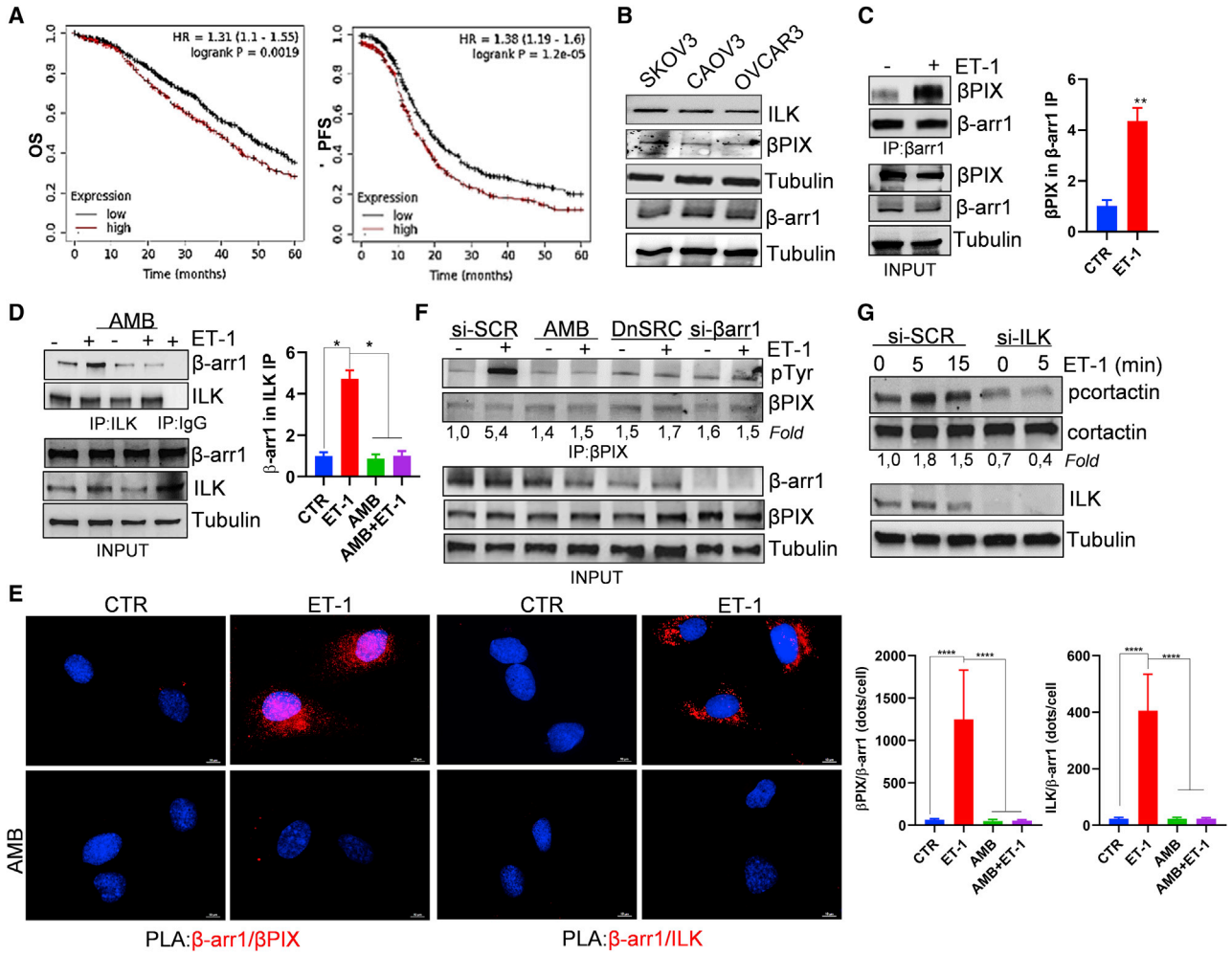

Figure 1. ILK/βPIX interacts with β-arr1 in SOC cells

(A) Kaplan-Meier analysis of overall survival (OS) or progression-free survival (PFS) curves in SOC patients with low or high ET_AR (*EDNRA*)/ILK expression.

(B) Representative western blot (WB) analysis of ILK, βPIX, and β-arr1 expression in indicated cell lines.

(C) Lysates of OVCAR3 cells stimulated with ET-1 (100 nM) for 30 min were immunoprecipitated (IP) with anti-β-arr1 Ab. IPs and inputs were analyzed for WB for βPIX and β-arr1 expression. Histograms indicate means ± SD of the average band intensity of βPIX in β-arr1 IP normalized to inputs (fold changes versus CTR); n = 3, t test, Welch correction.

(D) Lysates of SKOV3 cells stimulated with ET-1 and/or Ambrisentan (AMB) (1 μM) for 30 min were IP with anti-ILK Ab or immunoglobulin G (IgG). IPs and inputs were subjected to WB for β-arr1 and ILK expression. Histograms indicate means ± SD of the average band intensity of β-arr1 in ILK IP normalized to inputs (fold changes versus CTR). n = 3, one-way ANOVA, Tukey post hoc analysis.

(E) Representative image of PLA detection of βPix and β-arr1 or ILK and β-arr1 complexes in SKOV3 cells stimulated with ET-1 and/or AMB (30 min). The red signal represents positive PLA reaction, and DAPI staining (blue) highlights the nucleus. Scale bar, 10 μm. Histograms, means ± SD of PLA dots per nucleus from signals observed in about 30 cells chosen randomly in 5 different fields; n = 3. One-way ANOVA, Tukey post hoc analysis.

(F) si-SCR, Dn-SRC, and si-β-arr1-transfected OVCAR3 cells stimulated with ET-1 and/or AMB for 30 min were IP with anti-βPIX. IPs and inputs were subjected to WB for phospho-tyrosine (pTyr) and βPIX expression.

(G) si-SCR and si-ILK-transfected SKOV3 cells stimulated by ET-1 for indicated times were subjected to WB for phospho-cortactin (pcortactin) and cortactin. For (F) and (G), the fold change of pTyr/βPIX or pcortactin/cortactin with respect to control is reported. n = 3. For each WB, Tubulin was used for loading control. See also Figures S1 and S2.

βPIX might be phosphorylated on tyrosine 442 in response to growth factors and in an Src-dependent manner to promote Rho GTPase activity and cell motility (Feng et al., 2010). Considering that β-arr1 interacts with Src to regulate its activation (Luttrell et al., 1999; Imamura et al., 2001; Rosanò et al., 2009), we tested whether the ET-1-driven β-arr1/Src complex might control βPIX phosphorylation. ET-1 promotes tyrosine phosphorylation of βPIX, while this effect is lost in cells transfected with si-β-arr1 or with a plasmid expressing dominant-negative Src, or upon treatment with ambrisentan (Figure 1F). Moreover, the effect of silencing of β-arr1 can be rescued by the expression of β-arr1-FLAG (Figure S2D), further supporting the role of β-arr1/Src in ET-1-dependent phosphorylation/activation of βPIX. β-arr1/Src promotes ET-1-dependent tyrosine phosphorylation of cortactin

(Di Modugno et al., 2018), considered a key molecular switch promoting the invadopodia maturation into degradative structures (Oser et al., 2009; Mader et al., 2011). Therefore, we tested the effect of ILK on cortactin. While ET-1 promotes tyrosine phosphorylation of cortactin, silencing of ILK inhibits this effect in both SKOV3 and OVCAR3, implying ILK as an upstream regulator of cortactin (Figures 1G and S2E).

Overall, these data establish a molecular association between ILK/βPIX and β-arr1 taking place in SOC cells in an ET-1-dependent manner, which influences phosphorylation/activation of βPIX and cortactin, in virtue of the ability of β-arr1 to regulate Src activity.

ILK/βPIX/β-arr1 acts as a mediator of ET-1-driven Rac3 activity

Recent findings pointed to a prominent role of βPIX in orchestrating Rac3 GTPase activity, acting as a central node connecting signaling from growth factors and adhesion complexes at invadopodia (Donnelly et al., 2017; Rosenberg et al., 2017). Considering the implication of Rac3 in tumor progression (de Curtis, 2019), we compared the differences in Rac3 expression between SOC tissues and paired healthy tissues from three independent bioinformatics databases. Analysis from the GENT2 database identified a significantly higher *RAC3* expression in SOC tissues compared to normal ovarian tissues (Figure 2A). Moreover, *RAC3* is upregulated by at least 4-fold in 43 cases of SOC compared with 10 samples of normal peritoneum, according to the Yoshihara Ovarian Statistics data from the Oncomine database (https://www.oncomine.org/) (Figure 2B). Besides, the GEPIA (Gene Expression Profiling Interactive Analysis) dataset, used to compare the mRNA expression between tumor and normal tissues matching TCGA and GTEx data, further showed that the expression level of *RAC3* mRNA was higher in the tumor than in normal tissues (Figure S3A). These findings suggest that the role of Rac3 in SOC progression deserves to be further elucidated.

The GSE14407 dataset downloaded from the Gene Expression Omnibus (GEO) database also confirmed that *RAC3* mRNA expression was higher in ovarian cancer cells in comparison to normal ovarian surface epithelial (OSE) cells (Figure S3B). Our SOC cell lines express Rac3 at both mRNA and protein levels (Figures 2C and 2D). Then, we analyzed the changes in the activation status of Rac3 upon ET-1 challenge and the role of ILK/β-arr1/βPIX complex. As shown by pull-down assays, ET-1 enhanced Rac3 activation within 5 min in all cell lines (Figures 2E–2G and S3C–S3E). Silencing of β-arr1 or ET_AR, as well as treatment with ambrisentan, but not with BQ788, dramatically impaired Rac3 activation (Figures 2E, 2G, and S3C–S3E). The inhibitory effect in ET-1-induced Rac3 activation was also observed in cells silenced for either ILK or βPIX (Figures 2E and 2F). Moreover, overexpression of ET_AR or β-arr1 rescued the effect of their silencing (Figures S3D and S3E). Altogether these data demonstrate that ET-1-dependent Rac3 activity is related to the ET_AR/β-arr1/ILK axis that requires the GEF activity of βPIX.

To uncover the detailed signaling pathways driven by ILK/βPIX/Rac3 molecular complex, we focused on PAK1 in the group I class of PAK family since βPIX is involved in activation of PAK and LIM domain kinases to inactivate cofilin and PAK1 regulates invadopodium at different levels (Jeannot et al., 2017; Nicholas et al., 2019; Williams et al., 2019; Gasparski et al., 2019). ET-1 enhanced phosphorylation of PAK1 at threonine 423 within its catalytic domain, a residue critical to its kinase activity (Figures 2H, 2I, and 2J). Silencing of βPIX or Rac3 or upstream ILK reduced ET-1-induced PAK1 phosphorylation (Figures 2I and 2J), indicating that βPIX/Rac3 serves as intermediate in ILK-dependent PAK1 activation. Cofilin-dependent actin polymerization is required for invadopodia maturation (Oser et al., 2009) and ET_AR/β-arr1 participates in the confinement of actin polymerization in invadopodia by inhibiting cofilin activity (Semprucci et al., 2016). While ET-1 induced phosphorylation/inactivation of cofilin on Ser3, silencing of ILK, βPIX, or Rac3 impaired this effect (Figures 2I and 2J). The silencing of ILK can be rescued by overexpression of ILK on phosphorylation of PAK1 and cofilin (Figure 2J), suggesting that ILK is a mediator of ET-1 in regulating cofilin signaling through PAK1.

The ET-1-dependent β-arr1/ILK/Rac3 axis regulates degradative activity at invadopodia

We then evaluated whether ILK/βPIX/Rac3 signaling contributes to ET-1-dependent invadopodia regulation. As shown in Figure 3, while ET-1 promotes the co-localization of cortactin with F-actin in both SKOV3 and OVCAR3 cells, silencing of ILK inhibited this interaction, indicating potential involvement of ILK/Rac3 signaling in the ET-1-regulated invadopodium protein recruitment. Since cancer cell lines might exhibit an adhesion ring formation around invadopodia consisting of adhesion components, such as paxillin and vinculin, and ILK plays a role in adhesion ring formation and maturation, we evaluated the localization of paxillin related to that of the invadopodium-specific marker cortactin. As shown by confocal laser scanner microscopy (CLSM) analysis in both OVCAR3 and SKOV3 cells, cortactin appears diffuse in the cytoplasm, and paxillin-positive structures are evident at the periphery of the cells. In ET-1-treated cells, a significant number of discrete paxillin-cortactin positive structures are present in the perinuclear region of the cells, an effect that was absent upon silencing of either ILK or Rac3, as well as upon ambrisentan treatment (Figures S4 and S5). To test the role of ILK as a mediator of ET_AR-driven invadopodia function and ECM degradation, we evaluated the ability of cells to produce ventral actin protrusions with degradative activity by gelatin degradation assays. ET-1 stimulation significantly increased the ability of cells to degrade the gelatin in all cell lines tested (Figure 4; Figures S6–S8). CLSM images show that paxillin-rich protrusions containing discrete cortactin spots (Figure 4), as well as F-actin/cortactin protrusions (Figures S6 and S8), protrude through the pores by actively degrading the ECM. A 3D-reconstruction model of selected regions with matrix holes indicated co-localization of paxillin with cortactin or cortactin with F-actin to or in the proximity of ECM-degrading invadopodia structures (Figure 4; Figures S6–S8). Treatment with ambrisentan or silencing of ILK or Rac3 or βPIX completely abolished the ET-1-driven effects (Figure 4; Figures S6–S8), demonstrating that ILK/βPIX/Rac3 signaling is a critical route in the ET-1-driven invadopodia process, by coordinating adhesion and degradative activities at invadopodia.

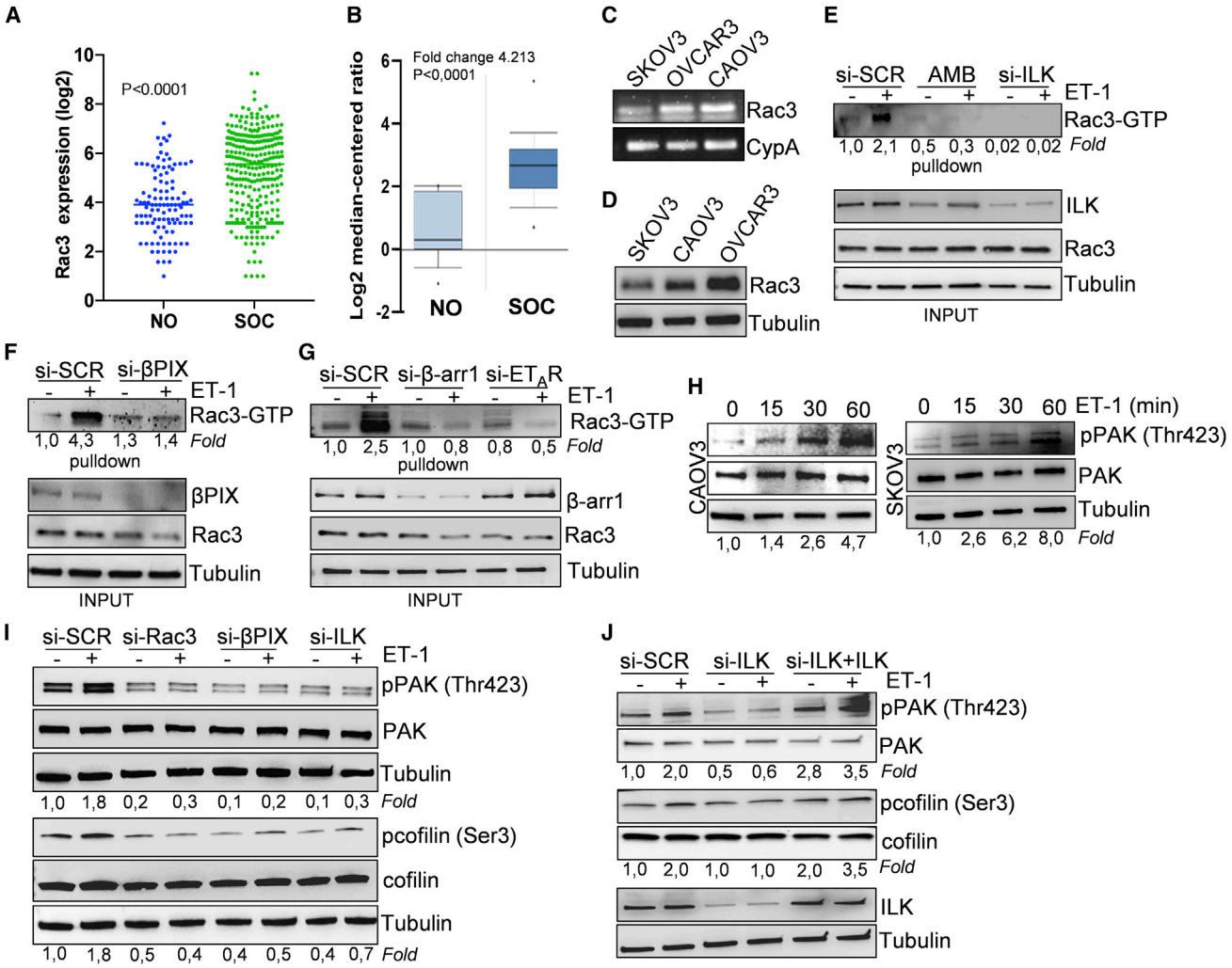

Figure 2. ET-1 regulates Rac3 activity through ILK/βPIX/β-arr1

(A) *RAC3* (Rac3) mRNA expression in normal ovarian tissues (NO, n = 110 samples) and SOC tissues (n = 285 samples) (GENT2 database). Mann-Whitney test.

(B) Oncomine data showing *RAC3* expression in SOC and normal tissues (NO). Mann-Whitney test.

(C) Representative RT-PCR analysis showing *RAC3* mRNA levels in indicated cell lines. CypA, loading control.

(D) Representative WB analysis of Rac3 expression in indicated cell lines.

(E) PAK-PBD-GST beads were used to pull down Rac3-GTP from si-SCR and si-ILK-transfected CAOV3 cells stimulated with ET-1 and/or AMB for 5 min.

(F) PAK-PBD-GST beads were used to pull down Rac3-GTP from si-SCR and si-βPIX-transfected OVCAR3 cells stimulated with ET-1 for 5 min.

(G) PAK-PBD-GST beads were used to pull down Rac3-GTP from si-SCR, si-β-arr1, and si-ET_AR-transfected OVCAR3 cells stimulated with ET-1 for 5 min. For (E)–(G), pull-down and input samples were analyzed by WB. The fold change of Rac3-GTP/Rac3 versus control is reported. n = 3.

(H) Lysates of cells stimulated with ET-1 were analyzed for phospho-PAK (pPAK) (Thr423) and PAK expression.

(I) si-SCR, si-Rac3, si-βPIX, and si-ILK-transfected OVCAR3 cells stimulated with ET-1 (60 min) were analyzed for WB for pPAK1, PAK1, phospho-cofilin (p-cofilin) (Ser3), and cofilin expression.

(J) SKOV3 cells transfected with si-SCR or si-ILK and co-transfected with ILK wild type (WT) and stimulated by ET-1 for 60 min were analyzed for WB for pPAK1, PAK1, p-cofilin, and cofilin expression.

For (H), (I), and (J), the fold change of pPAK1/PAK1 and p-cofilin/cofilin versus control is reported. n = 3. For each WB, Tubulin was used for loading control. See also Figure S3.

To more specifically test the requirement of ILK-dependent signaling for the ability of SOC cells to proteolytically cleave surrounding collagen fibers and invade, we cultured cells in droplets of polymerized collagen I and assessed pericellular collagenolysis by using the neoepitope Col1-3/4C antibody that recognizes the collagenase-cleaved fragment of collagen I (Wolf et al., 2007; Monteiro et al., 2013). In SKOV3 cells embedded in type I collagen, ET-1 significantly induces pericellular collagen degradation as indicated by the staining from Col1-3/4C, while this signal is strongly reduced upon treatment with ambrisentan or after depletion of ILK or Rac3 (Figure 5A).

MT1-MMP is considered the dominant protease accumulating at invadopodia and critical for focal degradation of ECM to these sites (Ferrari et al., 2019). Considering that phosphorylation of

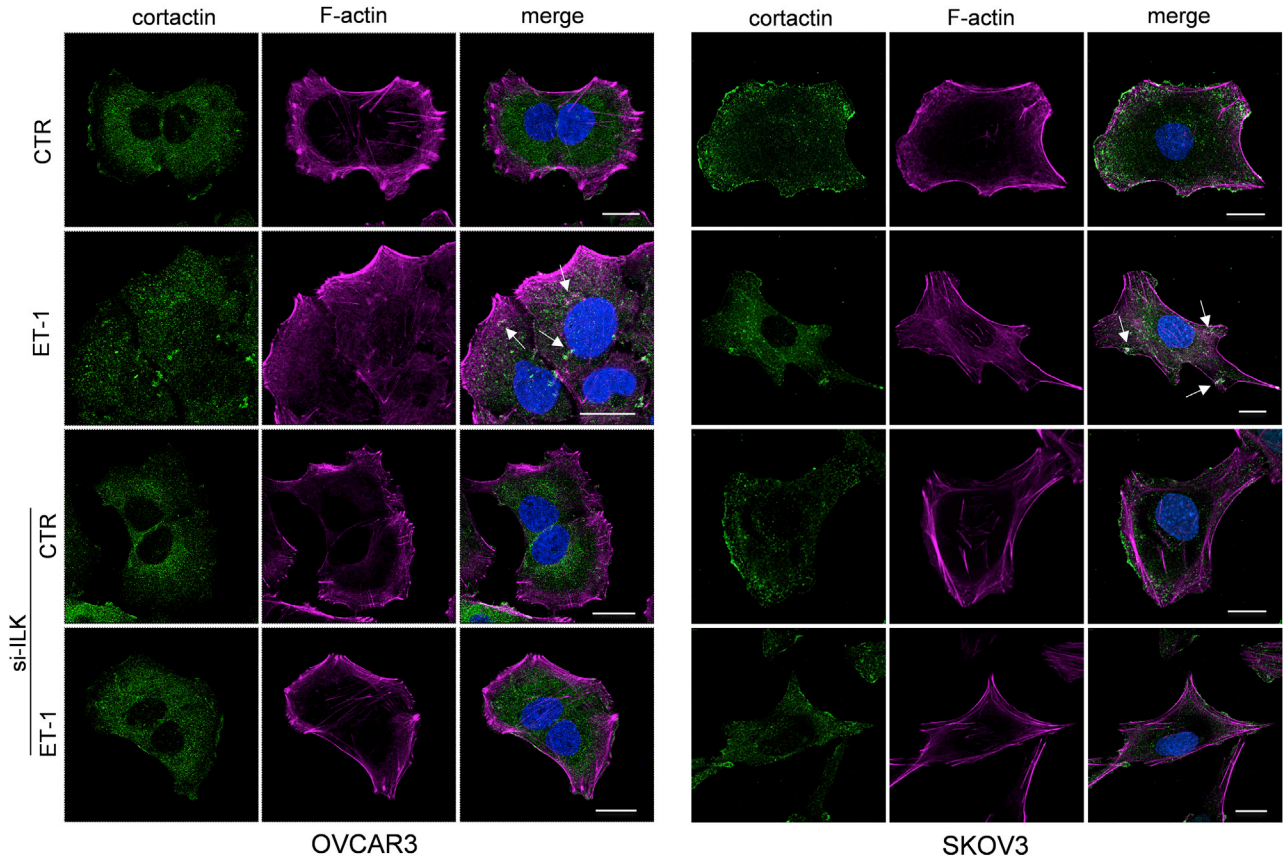

Figure 3

Figure 3. ET-1R/ILK signaling regulates the interaction of paxillin with cortactin

A confocal laser scanning microscopy (CLSM) analysis of OVCAR3 (left panels) or SKOV3 (right panels) cells transfected with si-ILK and stimulated with ET-1 for 6 h and then stained for cortactin (green) and F-actin (magenta) detection. Co-localization is shown in merged images, detected in white (arrows). Nuclei are reported in blue (DAPI). Scale bar, 20 μm. See also Figures S4 and S5.

MT1-MMP on Thr567 regulates its activity promoting adhesion and invasion of both meso-mimetic cultures and collagen by SOC cells (Yang et al., 2017) and that MT1-MMP is an ILK substrate (Bruney et al., 2016), we tested whether ILK phosphorylates MT1-MMP upon ET-1 axis activation. As shown in Figures 5B and S3F, phosphorylation of MT1-MMP is evident downstream of ET-1 stimulation, while silencing of ILK or ambrisentan treatment hampered this effect, indicating that ET-1/ILK regulates MT1-MMP activity. This effect most likely favors the cleavage and activation of MMP-2 and -9, since gelatin zymography assays showed that ILK silencing negatively affects the ability of ET-1 to promote their expression and secretion (Figure S3G).

Cancer cells use invadopodia to breach basement membranes and invade mesenchymal tissues. To link ILK-dependent invadopodia to cell invasion, we performed inverted invasion assays, where cells were allowed to invade into a plug composed of fibrillar collagen-I. Importantly, while cells stimulated with ET-1 invade efficiently into collagen I, this effect is almost lost when cells were silenced for ILK or Rac3 or were treated with ambrisentan (Figure 5C). This was also the case for cells that were grown as spheroids and tested for the capacity to invade in a 3D type I collagen matrix. As compared with multicellular spheroids of ET-1-treated cells, invasion of β-arr1/ILK/Rac3-silenced spheroids was decreased by ~40% similar to ambrisentan-treated cells (Figure S9A). In line with the above results, the ET-1-induced cell invasion is impaired upon silencing of ILK, βPIX, Rac3, β-arr1, and ET_AR or upon treatment with ambrisentan in transwell invasion assays, while overexpression of ET_AR or β-arr1 rescued the effect of their silencing (Figures S9B and S9C). Altogether, these data indicate that the invadopodium formation and pericellular collagen degradation require the components of the ILK/Rac3 axis to enhance the invasive potential of SOC cells.

Ovarian cancer cell interaction with mesothelial cells and invasion are regulated by ET-1-dependent ILK/β-arr1/Rac3 signaling

Since during SOC spread, tumor cells attach to and invade through the mesothelium—an epithelial-like monolayer lining the organs of the abdominal cavity (Lengyel, 2010; Yeung et al., 2015)—we tested the ability of cells to adhere to mesothelial cells and to migrate through mesothelial monolayer *in vitro*.

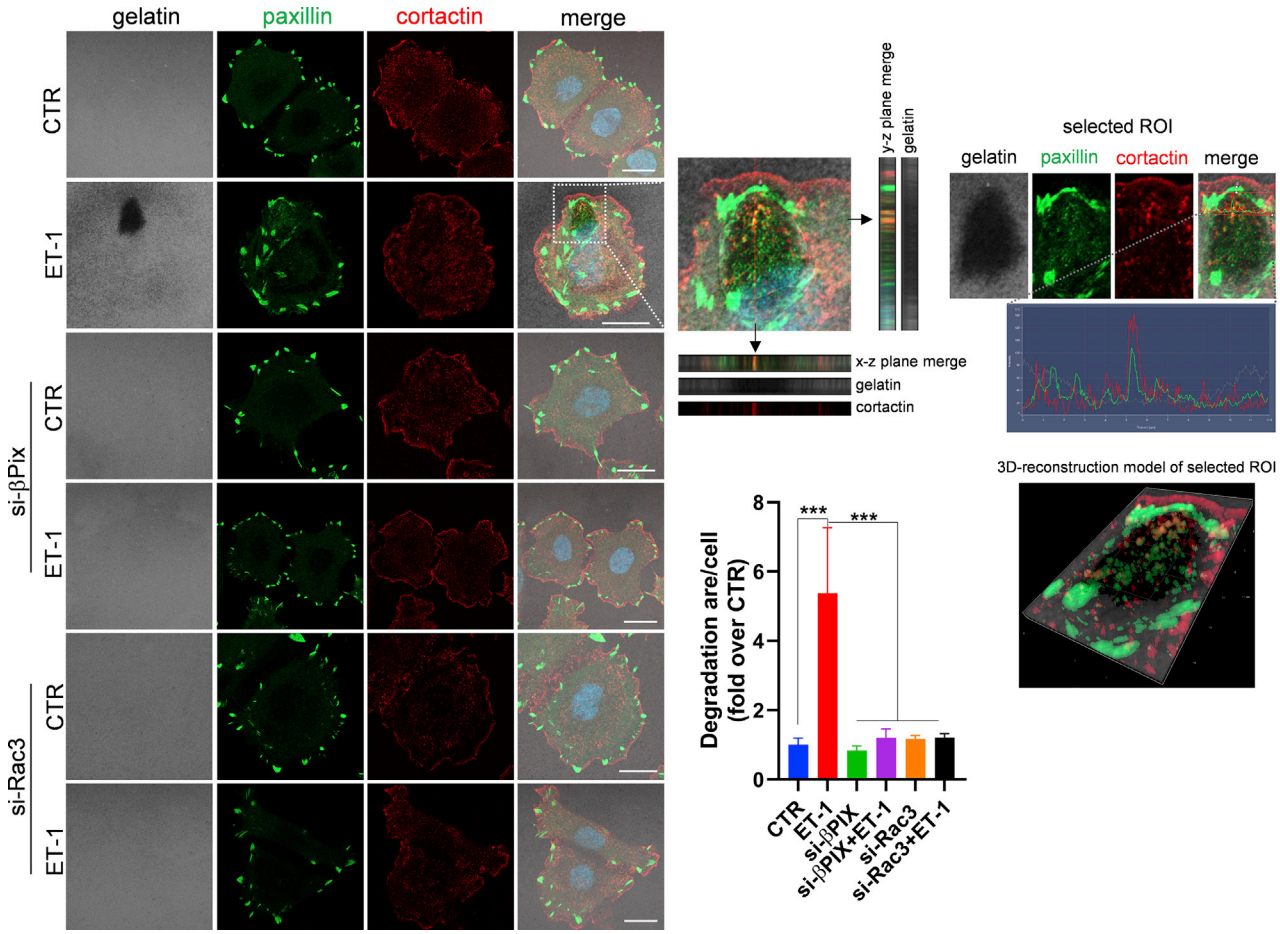

Figure 4. ET-1-driven invadopodia function is mediated by ILK/βPIX/Rac3 signaling

CLSM analysis of OVCAR3 cells, transfected with si-SCR, si-βPIX, or si-Rac3, plated onto gelatin and treated with ET-1 (48 h). Cells were stained for paxillin (green) and cortactin (red). Gelatin was reported in pseudo color gray and nuclei in blue (DAPI). Co-localization is shown in merged images. Orthogonal views (y-z plane; x—z plane) indicate areas of degraded gelatin with co-localized paxillin and cortactin (arrows). Right, separate channels and merged images of the selected ROI and the histogram profiles of paxillin/cortactin/gelatin signals in the line drawn. A 3D-reconstruction model showing paxillin/cortactin complexes (detected in yellow) in the matrix-degrading area is shown. Scale bar, 20 μm. Histograms, means ± SD of normalized degradation area percentage of cells). n = 3, one-way ANOVA, Tukey post hoc analysis. See also Figures S6–S8.

As shown by a quantitative evaluation of the adhesion of cancer cells to the primary mesothelial cell monolayer, the number of cells adhering to the monolayer significantly increased upon ET_AR activation, as confirmed by the inhibitory effect of ambrisentan (Figures 6A and S10A). Silencing of ILK, βPIX, or Rac3 inhibited this process (Figures 6A and S10A), confirming that ILK/βPIX/Rac3 molecular signaling controls the adhesion to mesothelial cells.

To test the transmesothelial migration ability, fluorescently labeled cells invading across the mesothelial cells were fixed and counted. While ET-1 significantly promoted transmesothelial movement through meso-mimetic cultures, silencing of ILK, βPIX, or Rac3 or ambrisentan treatment significantly reduced this effect (Figures 6B and S10B), further supporting the role of ET-1-dependent ILK/βPIX/Rac3 signaling to facilitate the communication between SOC and mesothelial cells, supporting cell invasion. Of note, ET-1-dependent invadopodia are most likely involved in this process since silencing of TKS5 or MT1-MMP inhibited this effect (Figure 6B).

Ambrisentan suppresses intraperitoneal seeding and metastasis in SOC xenografts

To assess the significance of ET_AR signaling in regulating intraperitoneal seeding and metastatic behavior *in vivo* and to evaluate the inhibition of ET_AR-dependent signaling as a therapeutic opportunity to control metastatic colonization, mice were intraperitoneally injected with SKOV3 cells stably expressing luciferase, to mimic some aspects of ovarian cancer cell seeding on the peritoneal surfaces, representing typical metastatic sites observed in patients with an advanced stage of the disease.

For *in vivo* adhesion assays, untreated or ambrisentan-pretreated tumor cells were i.p. injected, and abdominal organs (liver, kidneys, intestine and mesentery, spleen with pancreas, and omentum) were excised. Based on the *ex vivo* bioluminescence (BLI) value from luciferase-expressing cells, significantly

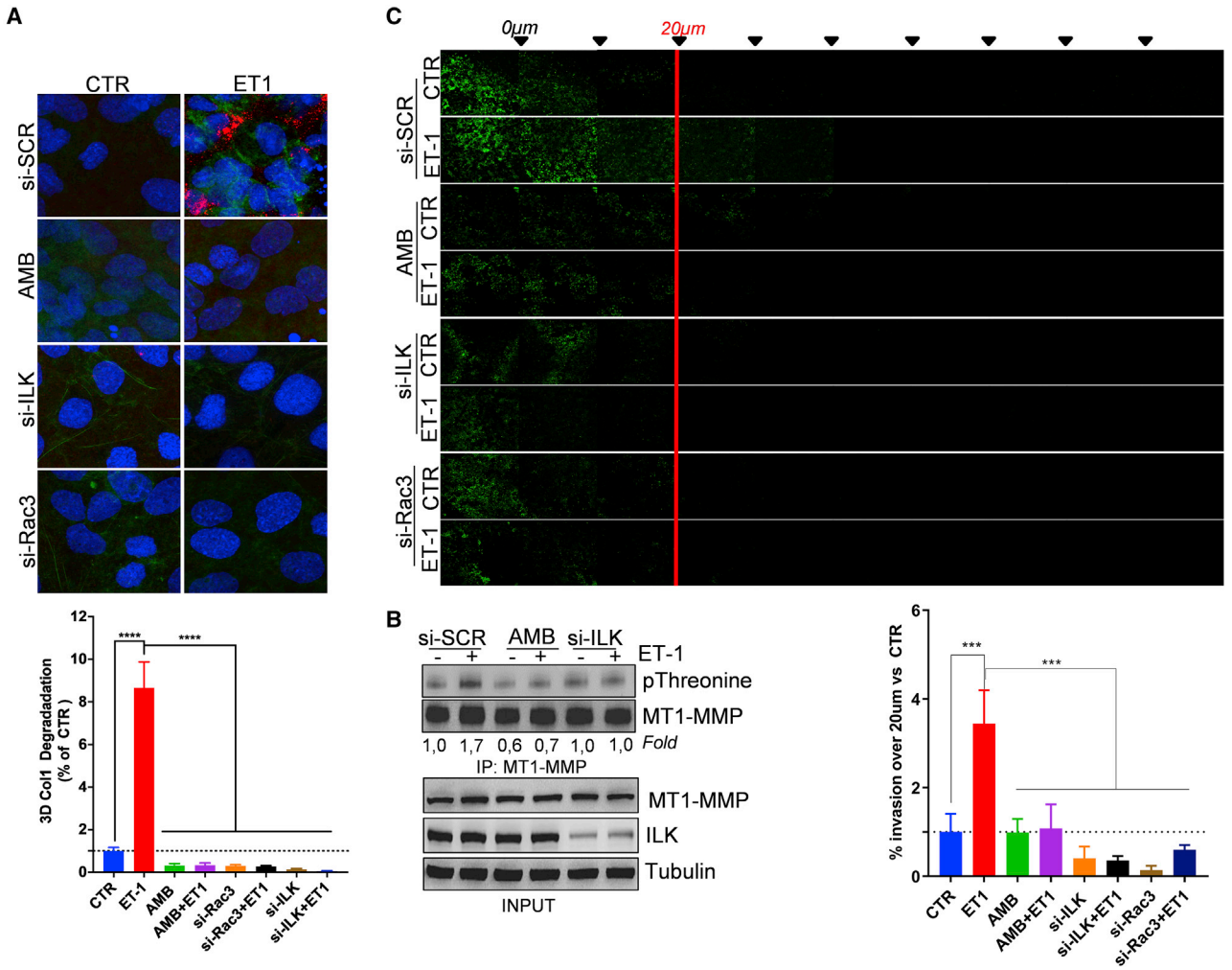

Figure 5. ET_AR/ILK/Rac3 promotes cleavage of collagen I, MT1-MMP phosphorylation, and cell invasion

(A) Pericellular collagenolysis by SKOV3 cells transfected with si-SCR, si-ILK, or si-Rac3 and treated with ET-1 and/or AMB, measured as the mean intensity of Col1-3/4C (red)/collagen I (green) signal per cell ± SD. DAPI staining (blue) highlights the nucleus. Histograms, the mean ± SD, n = 2. one-way ANOVA, Tukey post hoc analysis.

(B) si-SCR and si-ILK-transfected SKOV3 cells stimulated with ET-1 and/or AMB for 30 min were IP with anti-MT1-MMP Ab. IPs and inputs were subjected to WB for pThr and MT1-MMP expression and Tubulin for loading control. The fold change of pThr/MT1-MMP versus control is reported. n = 3.

(C) si-SCR, si-ILK, and si-RAC3 SKOV3 cells treated with ET-1 and/or AMB were allowed to invade type I collagen plugs in an inverted invasion assay (48 h). Cells were stained with PKH67, and serial optical sections (10-μm intervals) were acquired. The invasion was measured by dividing the sum of signal intensity of all slides beyond 20 μm (invading cells) by the sum of the intensity of all slides (total cells). n = 2, one-way ANOVA, Tukey post hoc analysis.

See also Figures S3 and S9.

more tumor cells attached to the mesentery, peritoneum, and omentum in the control group compared with the ambrisentan-treated group (Figure 7A).

To examine whether ambrisentan therapy can inhibit intraperitoneal dissemination, mice were treated with vehicle or ambrisentan for 5 weeks, and tumor cell propagation in the peritoneal cavity of mice was evaluated by BLI images every 3 days. BLI analyses revealed that ambrisentan significantly inhibited intraperitoneal spreading (Figure 7B). After sacrifice, peritoneal metastatic organs were examined, and several nodules were recorded. Metastases spread across the abdominal cavities of the mice, including the kidney, spleen, omentum, intestine, mesentery, and the abdominal wall. Ambrisentan markedly reduced the number of metastatic lesions in the abdomen (Figure 7C). The evaluation of the changes in the expression of invadopodia effectors in different metastatic nodules demonstrated a reduced expression of Rac3 and cortactin in nodules from ambrisentan-treated mice (Figure 7D). These data strongly suggest a therapeutic window where ambrisentan might be used in the treatment of SOC metastasis.

DISCUSSION

Identifying regulatory mechanisms of SOC progression is important toward developing therapeutic tools against pre-metastatic

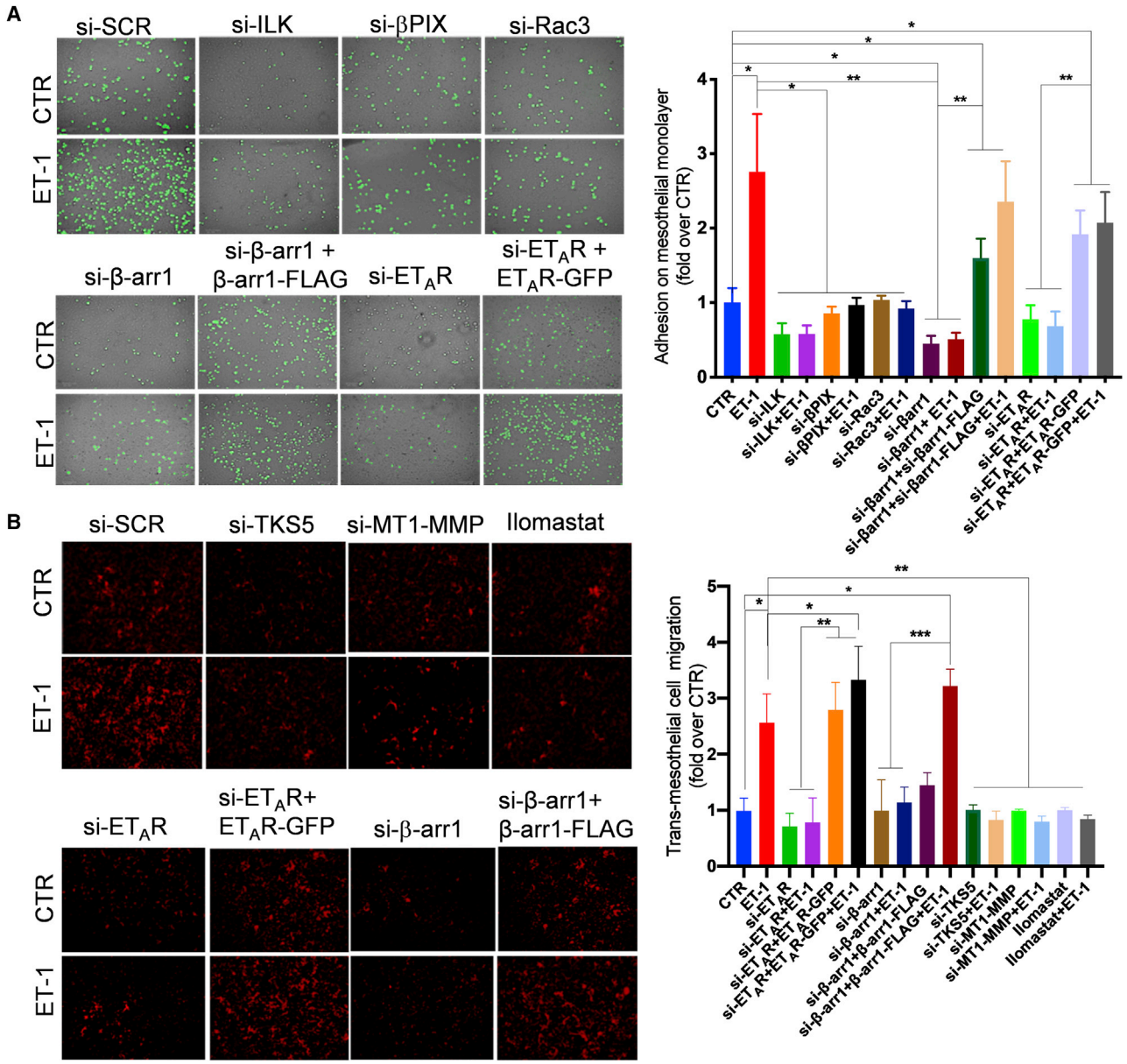

Figure 6. ILK/βPIX/Rac3 signaling enhances the ability of SOC cells to adhere to and migrate across monolayered human mesothelial cells

(A) SKOV3 cells (green), transfected with si-SCR, si-βPIX, si-ILK, and si-Rac3 or, when indicated, with si-β-arr1 and si-ET_AR and/or co-transfection with mock or β-arr1-FLAG or ET_AR-GFP, respectively, were seeded into a monolayer of mesothelial cells (gray) and stimulated with ET-1 and/or AMB for 30 min. Images of adherent cells were captured. Histograms means ± SD from the quantification of signals in 15 different fields. n = 3, one-way ANOVA, Tukey post hoc analysis.

(B) SKOV3 cells (red), transfected with si-SCR, si-TKS5, and si-MT1-MMP or, when indicated, with si-β-arr1 and si-ET_AR and/or co-transfection with mock or β-arr1-FLAG or ET_AR-GFP, respectively, were applied into the upper chamber with a monolayer of mesothelial cells on a fibronectin-coated membrane and stimulated with ET-1 and/or AMB and/or Ilomastat for 30 min. After 12 h, cells migrated through the mesothelial layer, and fibronectin and membrane pores were photographed. Histograms means ± SD from the quantification of signals in 15 different fields. n = 3, one-way ANOVA, Tukey post hoc analysis.

See also Figure S10.

cancer. Metastatic progression requires the successful completion of sequential steps, and the invasion of cancer cells through the ECM is a prerequisite of the metastasis formation. To achieve efficient motility, cancer cells might employ protease-secreting invadopodia, enabling them to break the ECM and to disseminate and colonize secondary sites (Paterson and Courtneidge, 2018; Eddy et al., 2017; Leong et al., 2014). In this study, we provide a direct mechanism by which the ET_AR/β-arr1 pathway integrates adhesion and proteolytic signaling through ILK/Rac3 that allows cells to remodel ECM and invade. Mechanistically, we demonstrate that (1) concomitant high expression of ET_AR/ILK is a negative prognostic factor in SOC patients; (2) βPIX is a

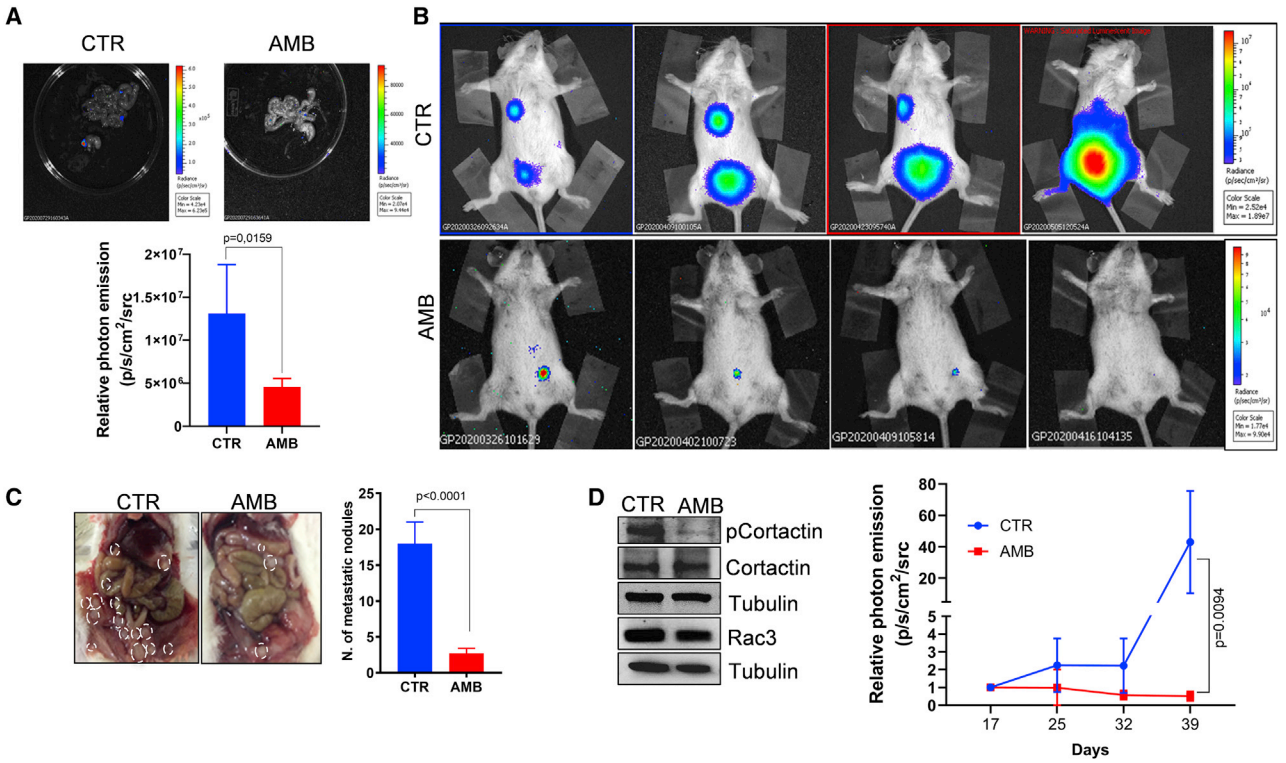

Figure 7. Ambrisentan inhibits peritoneal adhesion, metastatic dissemination, and invadopodia marker expression

(A) Bioluminescent images of SKOV3-Luc cells, untreated (CTR) or pretreated with Ambrisentan (AMB), on abdominal organs (n = 5 mice/group). The organs arranged are intestine and mesentery, spleen with pancreas, and omentum. The adherent cell aggregates were observed, and the luminescence was read and recorded. Data are presented as mean ± SD, n = 2, Mann-Whitney test.

(B) Bioluminescent images of i.p. SKOV3-Luc-injected mice, undergoing treatments for 5 weeks with 200 μL Metocell (vehicle, CTR) or 200 μL AMB (10 mg/kg, oral daily), both by oral gavage. Tumor burden was assessed on days 17, 25, 32, and 39 after tumor cell injection. Data are presented as mean ± SD, n = 2, Mann-Whitney test.

(C) Mice treated as in (B) were euthanized at the end of the treatment, and visible intraperitoneal nodules (indicated by white arrowheads) were photographed and counted. Data are presented as means ± SD, n = 2, Mann-Whitney test.

(D) Representative WB for Rac3, pCortactin, and cortactin expression in metastatic nodules. Tubulin was used for loading control.

new interactor of β-arr1 and ILK; (3) the ILK/βPIX/β-arr1 platform represents the means through which ET_AR controls the activity of Rac3 GTPase and cofilin, operating invadopodia-dependent ECM remodeling and cell invasion; (4) the signaling pathway between ET_AR and ILK/βPIX/Rac3 facilitates the interaction with mesothelial cells, favoring cell invasion and metastatic progression; and (5) ambrisentan inhibits adhesion and metastatic dissemination of SOC cells.

Invadopodia formation is a dynamic process requiring the combined and synergistic activity of ECM-modifying proteins with growth factors receptors and the interplay with tumor microenvironmental factors (Paterson and Courtneidge, 2018). Although the involvement of several growth factors in the assembly and function of invadopodia is emerging, how growth factor receptors interact with specific adapters and signaling molecules to drive formation and activation of these proteolytic structures, modifying the stroma to a permissive state to invasion, is not fully understood. In this context, our recent findings highlighted β-arr1 as the center of a regulatory complex at the interface of ET_AR signaling and invadopodia, in fine-tuning SOC cell invasion and metastasis (Rosanò and Bagnato, 2019). As a primary component of a core scaffold to direct spatiotemporal specificity of multi-protein complexes, β-arr1 controls the reorganization of the actin cytoskeleton to favor ECM degradation and transendothelial migration process (Semprucci et al., 2016; Di Modugno et al., 2012, 2018; Purayil and Daaka, 2018; Chellini et al., 2019). As previously reported, ILK might function as a bridge between proteolytic and adhesion signaling, since it resides in the same pathway of integrins to invadopodium-associated ECM degradation (Sakurai-Yageta et al., 2008), making ILK as an attractive signaling molecule to dissect in ET-1-dependent invadopodium activity. Previous studies demonstrated a cross-regulation between ET-1 and βPIX (Chahdi et al., 2005, Chahdi and Sorokin, 2006). Moreover, βPIX is considered a potent driver of invadopodia formation upon hypoxic stimulus (Md Hashim et al., 2013). Our findings highlight ILK as a key molecular partner modulating the emergence of invadopodia and provide a framework linking ET-1 and βPIX, involving ILK and β-arr1, to modulate the molecular switch of Rac3 from inactive to an active state, providing a mechanism connecting ILK to cytoskeleton dynamic and invadopodium-mediated cell invasion. Furthermore, these findings further

highlight the relevance of β-arr1 in invasion and metastasis via invadopodia regulation and, together with the described role of β-arr2 in invadopodia and metastatic progression (Li et al., 2009), reinforce the relevance of β-arrs as major hubs controlling GPCR signaling network in tumor progression.

In the family of Rho GTPases, while the role of Rac1 in cancer is well established, the implication of the closely related Rac3 is only recently becoming evident, resulting in its expression in different human tumors, including breast cancer, glioblastoma, prostate cancer, and lung adenocarcinoma (de Curtis, 2019). In the invadopodium context, Rac3 has been proposed as a driver of breast cancer invasion and metastasis formation (Donnelly et al., 2017; Rosenberg et al., 2017). Its activation is critical for integrin-mediated invadopodium adhesion to the ECM and delivery of MMPs for ECM proteolysis, representing an important node connecting growth factor signaling, such as that of epidermal growth factor receptor, with adhesion signaling at invadopodia (Donnelly et al., 2017). Our study uncovers a specific role of ILK/βPIX for activation of Rac3 and downstream of PAK1, linked to cofilin regulation. Although PAK1 localizes to invadopodia with opposite effects depending on the cellular context (Moshfegh et al., 2014; Jeannot et al., 2017; Williams et al., 2019; Nicholas et al., 2019), we hypothesize that activation of PAK1 downstream of ET-1/ILK/Rac3 can determine the balance between activation/inactivation of cofilin contributing to invadopodium life cycle and provide mechanistic insights into the role of ILK coupling adhesion and growth factor receptors during invasive activities. Besides, the loss of matrix degradation, as well as inhibition of MT1-MMP observed upon silencing of components of the ILK complex, suggests an additional function of ILK in invadopodia maturation and complements previous findings demonstrating the involvement of ILK/IQGAP1 in delivering MMPs to the plasma membrane (Sakurai-Yageta et al., 2008; Wickström et al., 2010; Branch et al., 2012). According to the well-demonstrated role of βPIX in orchestrating Rac3 activation only in the ring-like compartment (Donnelly et al., 2017) and consistent with the idea that the ring-like compartment is adhesion dependent (Branch et al., 2012), our findings suggest the importance of β-arr1/βPIX interaction in regulating Rac3 activation in a specific region of invadopodia and most likely for the correct delivery of proteases.

In patients with advanced SOC, tumor cells show a propensity to recur as an intraperitoneal metastatic disease by adhering and transmigrating to the mesothelial cells and subsequently inducing submesothelial ECM invasion (Lengyel, 2010). Our understanding of the biology of the ovarian tumor microenvironment has evolved quickly, discovering the tumor-promoting signaling between mesothelial and SOC cells actively participates in the establishment of the metastatic niche, and suggesting that controlling mediators of mesothelial/SOC cell interplay might represent a vulnerability in the treatment of this tumor (Kenny et al., 2015). According to previous data showing that ILK mediates ovarian cancer cell adhesion and invasion of meso-mimetic cultures (Bruney et al., 2016), our findings integrate the idea that ILK and its interaction with β-arr1/βPIX, coupled to Rac3 activation and post-translational regulation of the MT1-MMP, might represent a novel mechanism in the establishment of productive interactions of SOC cells to monolayer surfaces, as a prerequisite to bypass the mesothelial barrier, and finally to support an invadopodium-mediated invasion. These findings complement the importance of Rac3 in balancing ECM adhesion and ECM degradation to a functional role during the metastatic cascade (Donnelly et al., 2017).

The beneficial effects of ET_AR/ILK signaling in invasive protrusions and tumor-stroma interactions appear to be dependent by β-arr1/βPIX molecular complex, as evident by the impairment of these processes *in vitro* after ablation of single components. Of note, our results also indicate a potential of a drug-repurposing strategy using ambrisentan, a selective ET_AR antagonist approved by the FDA and EMA for the treatment of pulmonary hypertension, to interfere with the ET_AR/β-arr1 axis to limit the metastatic potential of SOC cells. Ambrisentan at the low dosage is effective in inhibiting both the adhesion to intraperitoneal organs and the spread of SOC cells, by controlling also invadopodia effectors. In line with our results, recent findings showed that ambrisentan is effective in decreasing metastasis into the lungs and liver from breast cancer cells, associated with the enhancement in animal survival (Kappes et al., 2020). In our previous studies, we evaluated the effect of ET_BR antagonism along with ET_AR antagonism in ovarian cancer cells (Rosanò et al., 2005, 2014; Tocci et al., 2019) using either specific ET_BR antagonist or dual ET-1R antagonist. According to data obtained in this work, it seems that the best means to target the ET-1 axis in ovarian cancer patients would be to use an ET_AR-specific antagonist, capable of blocking critical pathways involved in cancer invasion. Indeed, significant inhibition of tumor growth, EMT, invasion, and metastatic progression has been observed targeting ET_AR, while ET_BR blockade can enhance anti-tumor immune cell recruitment and inhibit tumor vascularization (Buckanovich et al., 2008; Kandalaft et al., 2009; Coffman et al., 2013). Altogether these findings indicate that targeting ET_AR harnessing the metastatic ability of SOC cells is an avenue to be explored.

Previous studies using primary and metastatic ovarian carcinomas showed that both ET-1 receptors are expressed, and, in particular, ET_AR is strongly expressed in ovarian carcinoma cells, whereas ET_BR is mainly found in the endothelial cells of intratumoral vessels (Salani et al., 2000). Expression of ET-1 and ET_AR correlates with advanced stages of the disease associated with a poor prognosis (Rosanò et al., 2005, 2011). Accordingly, molecular indicators derived from bioinformatic analyses showing that high expression levels of ET_AR/ILK positively correlate with poor prognosis, conveying important prognostic information that might be translated in clinical situations, as predictive prognostic markers in SOC patients. Future experiments designed to explore the regulatory landscape of integrin-related signaling and its connection with the ET-1R/β-arr1/ILK axis might fully elucidate the integration of adhesion and proteolytic pathways in the pre-metastatic niche.

STAR★METHODS

Detailed methods are provided in the online version of this paper and include the following:

- KEY RESOURCES TABLE
- RESOURCE AVAILABILITY
  - Lead contact

SUPPLEMENTAL INFORMATION

Supplemental information can be found online at https://doi.org/10.1016/j.celrep.2021.108800.

ACKNOWLEDGMENTS

We gratefully acknowledge Aldo Lupo for excellent technical assistance and Maria Vincenza Sarcone for secretarial assistance. The research leading to these results has received funding from AIRC under IG 2018 - ID, 21372 project – PI L.R., and by grants from IRCCS Regina Elena National Cancer Institute to L.R. (Ricerca Corrente 2018-2019).

AUTHOR CONTRIBUTIONS

Conceptualization, L.R.; methodology, I.M. and V.C.; validation, I.M., V.C., and L.R.; formal analysis, F.S., A.Z., A.R., and L.R.; investigation, I.M., V.C., F.S., R.S., L.C., and A.Z.; writing – original draft, L.R.; writing – review & editing, F.S., A.R., A.B., and L.R.; visualization, I.M. and L.R.; supervision, L.R., funding acquisition, L.R.

DECLARATION OF INTERESTS

The authors declare no competing interests.

Received: April 21, 2020
Revised: January 2, 2021
Accepted: February 5, 2021
Published: March 2, 2021

REFERENCES

Ahmed, N., Riley, C., Oliva, K., Stutt, E., Rice, G.E., and Quinn, M.A. (2003). Integrin-linked kinase expression increases with ovarian tumour grade and is sustained by peritoneal tumour fluid. J. Pathol. *201*, 229–237.

Antelmi, E., Cardone, R.A., Greco, M.R., Rubino, R., Di Sole, F., Martino, N.A., Casavola, V., Carcangiu, M., Moro, L., and Reshkin, S.J. (2013). ß1 integrin binding phosphorylates ezrin at T567 to activate a lipid raft signalsome driving invadopodia activity and invasion. PLoS ONE *8*, e75113.

Badowski, C., Pawlak, G., Grichine, A., Chabadel, A., Oddou, C., Jurdic, P., Pfaff, M., Albigès-Rizo, C., and Block, M.R. (2008). Paxillin phosphorylation controls invadopodia/podosomes spatiotemporal organization. Mol. Biol. Cell *19*, 633–645.

Bagrodia, S., Taylor, S.J., Jordon, K.A., Van Aelst, L., and Cerione, R.A. (1998). A novel regulator of p21-activated kinases. J. Biol. Chem. *273*, 23633–23636.

Baird, D., Feng, Q., and Cerione, R.A. (2005). The Cool-2/α-Pix protein mediates a Cdc42-Rac signaling cascade. Curr. Biol. *15*, 1–10.

Beaty, B.T., Sharma, V.P., Bravo-Cordero, J.J., Simpson, M.A., Eddy, R.J., Koleske, A.J., and Condeelis, J. (2013). β1 integrin regulates Arg to promote invadopodial maturation and matrix degradation. Mol. Biol. Cell *24*, 1661–1675, S1–S11.

Bowen, N.J., Walker, L.D., Matyunina, L.V., Logani, S., Totten, K.A., Benigno, B.B., and McDonald, J.F. (2009). Gene expression profiling supports the hypothesis that human ovarian surface epithelia are multipotent and capable of serving as ovarian cancer initiating cells. BMC Med. Genomics *2*, 71.

Branch, K.M., Hoshino, D., and Weaver, A.M. (2012). Adhesion rings surround invadopodia and promote maturation. Biol. Open *1*, 711–722.

Bruney, L., Liu, Y., Grisoli, A., Ravosa, M.J., and Stack, M.S. (2016). Integrin-linked kinase activity modulates the pro-metastatic behavior of ovarian cancer cells. Oncotarget *7*, 21968–21981.

Buckanovich, R.J., Facciabene, A., Kim, S., Benencia, F., Sasaroli, D., Balint, K., Katsaros, D., O'Brien-Jenkins, A., Gimotty, P.A., and Coukos, G. (2008). Endothelin B receptor mediates the endothelial barrier to T cell homing to tumors and disables immune therapy. Nat. Med. *14*, 28–36.

Cabodi, S., del Pilar Camacho-Leal, M., Di Stefano, P., and Defilippi, P. (2010). Integrin signalling adaptors: not only figurants in the cancer story. Nat. Rev. Cancer *10*, 858–870.

Chahdi, A., and Sorokin, A. (2006). Endothelin 1 stimulates beta1Pix-dependent activation of Cdc42 through the G(salpha) pathway. Exp. Biol. Med. (Maywood) *231*, 761–765.

Chahdi, A., Miller, B., and Sorokin, A. (2005). Endothelin 1 induces beta 1Pix translocation and Cdc42 activation via protein kinase A-dependent pathway. J. Biol. Chem. *280*, 578–584.

Chellini, L., Caprara, V., Spadaro, F., Sestito, R., Bagnato, A., and Rosanò, L. (2019). Regulation of extracellular matrix degradation and metastatic spread by IQGAP1 through endothelin-1 receptor signalling in ovarian cancer. Matrix Biol. *81*, 17–33.

Coffman, L., Mooney, C., Lim, J., Bai, S., Silva, I., Gong, Y., Yang, K., and Buckanovich, R.J. (2013). Endothelin receptor-A is required for the recruitment of antitumor T cells and modulates chemotherapy induction of cancer stem cells. Cancer Biol. Ther. *14*, 184–192.

de Curtis, I. (2019). The Rac3 GTPase in Neuronal Development, Neurodevelopmental Disorders, and Cancer. Cells *8*, 1063.

DeFea, K.A. (2013). Arrestins in actin reorganization and cell migration. Prog. Mol. Biol. Transl. Sci. *118*, 205–222.

Destaing, O., Block, M.R., Planus, E., and Albiges-Rizo, C. (2011). Invadosome regulation by adhesion signaling. Curr. Opin. Cell Biol. *23*, 597–606.

Di Modugno, F., Iapicca, P., Boudreau, A., Mottolese, M., Terrenato, I., Perracchio, L., Carstens, R.P., Santoni, A., Bissell, M.J., and Nisticò, P. (2012). Splicing program of human MENA produces a previously undescribed isoform associated with invasive, mesenchymal-like breast tumors. Proc. Natl. Acad. Sci. USA *109*, 19280–19285.

Di Modugno, F., Caprara, V., Chellini, L., Tocci, P., Spadaro, F., Ferrandina, G., Sacconi, A., Blandino, G., Nisticò, P., Bagnato, A., and Rosanò, L. (2018). hMENA is a key regulator in endothelin-1/β-arrestin1-induced invadopodial function and metastatic process. Proc. Natl. Acad. Sci. USA *115*, 3132–3137.

Donnelly, S.K., Cabrera, R., Mao, S.P.H., Christin, J.R., Wu, B., Guo, W., Bravo-Cordero, J.J., Condeelis, J.S., Segall, J.E., and Hodgson, L. (2017).

Rac3 regulates breast cancer invasion and metastasis by controlling adhesion and matrix degradation. J. Cell Biol. *216*, 4331–4349.

Eddy, R.J., Weidmann, M.D., Sharma, V.P., and Condeelis, J.S. (2017). Tumor cell invadopodia: invasive protrusions that orchestrate metastasis. Trends Cell Biol. *27*, 595–607.

Engelman, M.d.F.B., Grande, R.M., Naves, M.A., de Franco, M.F., and de Paulo Castro Teixeira, V. (2013). Integrin-linked kinase (ILK) expression correlates with tumor severity in clear cell renal carcinoma. Pathol. Oncol. Res. *19*, 27–33.

Feng, Q., Baird, D., Yoo, S., Antonyak, M., and Cerione, R.A. (2010). Phosphorylation of the cool-1/beta-Pix protein serves as a regulatory signal for the migration and invasive activity of Src-transformed cells. J. Biol. Chem. *285*, 18806–18816.

Ferrari, R., Martin, G., Tagit, O., Guichard, A., Cambi, A., Voituriez, R., Vassilopoulos, S., and Chavrier, P. (2019). MT1-MMP directs force-producing proteolytic contacts that drive tumor cell invasion. Nat. Commun. *10*, 4886.

Gasparski, A.N., Wilson, J.T., Banerjee, A., and Beningo, K.A. (2019). The Role of PAK1 in the maturation of invadopodia during transient mechanical stimulation. Front. Cell Dev. Biol. *7*, 269.

Graff, J.R., Deddens, J.A., Konicek, B.W., Colligan, B.M., Hurst, B.M., Carter, H.W., and Carter, J.H. (2001). Integrin-linked kinase expression increases with prostate tumor grade. Clin. Cancer Res. *7*, 1987–1991.

Gyorffy, B., Lánczky, A., and Szállási, Z. (2012). Implementing an online tool for genome-wide validation of survival-associated biomarkers in ovarian-cancer using microarray data from 1287 patients. Endocr. Relat. Cancer *19*, 197–208.

Hoshino, D., Branch, K.M., and Weaver, A.M. (2013). Signaling inputs to invadopodia and podosomes. J. Cell Sci. *126*, 2979–2989.

Imamura, T., Huang, J., Dalle, S., Ugi, S., Usui, I., Luttrell, L.M., Miller, W.E., Lefkowitz, R.J., and Olefsky, J.M. (2001). β -Arrestin-mediated recruitment of the Src family kinase Yes mediates endothelin-1-stimulated glucose transport. J. Biol. Chem. *276*, 43663–43667.

Jean-Charles, P.Y., Kaur, S., and Shenoy, S.K. (2017). G protein-coupled receptor signaling through β-arrestin-dependent mechanisms. J. Cardiovasc. Pharmacol. *70*, 142–158.

Jeannot, P., Nowosad, A., Perchey, R.T., Callot, C., Bennana, E., Katsube, T., Mayeux, P., Guillonneau, F., Manenti, S., and Besson, A. (2017). $p27^{Kip1}$ promotes invadopodia turnover and invasion through the regulation of the PAK1/Cortactin pathway. eLife *6*, e22207.

Kandalaft, L.E., Facciabene, A., Buckanovich, R.J., and Coukos, G. (2009). Endothelin B receptor, a new target in cancer immune therapy. Clin. Cancer Res. *15*, 4521–4528.

Kappes, L., Amer, R.L., Sommerlatte, S., Bashir, G., Plattfaut, C., Gieseler, F., Gemoll, T., Busch, H., Altahrawi, A., Al-Sbiei, A., et al. (2020). Ambrisentan, an endothelin receptor type A-selective antagonist, inhibits cancer cell migration, invasion, and metastasis. Sci. Rep. *10*, 15931.

Kenny, H.A., Lal-Nag, M., White, E.A., Shen, M., Chiang, C.Y., Mitra, A.K., Zhang, Y., Curtis, M., Schryver, E.M., Bettis, S., et al. (2015). Quantitative high throughput screening using a primary human three-dimensional organotypic culture predicts in vivo efficacy. Nat. Commun. *6*, 6220.

Lengyel, E. (2010). Ovarian cancer development and metastasis. Am. J. Pathol. *177*, 1053–1064.

Leong, H.S., Robertson, A.E., Stoletov, K., Leith, S.J., Chin, C.A., Chien, A.E., Hague, M.N., Ablack, A., Carmine-Simmen, K., McPherson, V.A., et al. (2014). Invadopodia are required for cancer cell extravasation and are a therapeutic target for metastasis. Cell Rep. *8*, 1558–1570.

Li, T.T., Alemayehu, M., Aziziyeh, A.I., Pape, C., Pampillo, M., Postovit, L.M., Mills, G.B., Babwah, A.V., and Bhattacharya, M. (2009). Beta-arrestin/Ral signaling regulates lysophosphatidic acid-mediated migration and invasion of human breast tumor cells. Mol. Cancer Res. *7*, 1064–1077.

Luttrell, L.M., Ferguson, S.S., Daaka, Y., Miller, W.E., Maudsley, S., Della Rocca, G.J., Lin, F., Kawakatsu, H., Owada, K., Luttrell, D.K., et al. (1999). Beta-arrestin-dependent formation of beta2 adrenergic receptor-Src protein kinase complexes. Science *283*, 655–661.

Mader, C.C., Oser, M., Magalhaes, M.A., Bravo-Cordero, J.J., Condeelis, J., Koleske, A.J., and Gil-Henn, H. (2011). An EGFR-Src-Arg-cortactin pathway mediates functional maturation of invadopodia and breast cancer cell invasion. Cancer Res. *71*, 1730–1741.

Masi, I., Caprara, V., Bagnato, A., and Rosanò, L. (2020). Tumor cellular and microenvironmental cues controlling invadopodia formation. Front. Cell Dev. Biol. *8*, 584181.

McDonald, P.C., Fielding, A.B., and Dedhar, S. (2008). Integrin-linked kinase–essential roles in physiology and cancer biology. J. Cell Sci. *121*, 3121–3132.

Md Hashim, N.F., Nicholas, N.S., Dart, A.E., Kiriakidis, S., Paleolog, E., and Wells, C.M. (2013). Hypoxia-induced invadopodia formation: a role for β-PIX. Open Biol. *3*, 120159.

Monteiro, P., Rossé, C., Castro-Castro, A., Irondelle, M., Lagoutte, E., Paul-Gilloteaux, P., Desnos, C., Formstecher, E., Darchen, F., Perrais, D., et al. (2013). Endosomal WASH and exocyst complexes control exocytosis of MT1-MMP at invadopodia. J. Cell Biol. *203*, 1063–1079.

Moshfegh, Y., Bravo-Cordero, J.J., Miskolci, V., Condeelis, J., and Hodgson, L. (2014). A Trio-Rac1-Pak1 signalling axis drives invadopodia disassembly. Nat. Cell Biol. *16*, 574–586.

Murphy, D.A., and Courtneidge, S.A. (2011). The 'ins' and 'outs' of podosomes and invadopodia: characteristics, formation and function. Nat. Rev. Mol. Cell Biol. *12*, 413–426.

Nicholas, N.S., Pipili, A., Lesjak, M.S., and Wells, C.M. (2019). Differential role for PAK1 and PAK4 during the invadopodia lifecycle. Small GTPases *10*, 289–295.

Nobles, K.N., Guan, Z., Xiao, K., Oas, T.G., and Lefkowitz, R.J. (2007). The active conformation of beta-arrestin1: direct evidence for the phosphate sensor in the N-domain and conformational differences in the active states of beta-arrestins1 and -2. J. Biol. Chem. *282*, 21370–21381.

Oser, M., Yamaguchi, H., Mader, C.C., Bravo-Cordero, J.J., Arias, M., Chen, X., Desmarais, V., van Rheenen, J., Koleske, A.J., and Condeelis, J. (2009). Cortactin regulates cofilin and N-WASp activities to control the stages of invadopodium assembly and maturation. J. Cell Biol. *186*, 571–587.

Parekh, A., and Weaver, A.M. (2016). Regulation of invadopodia by mechanical signaling. Exp. Cell Res. *343*, 89–95.

Park, S.J., Yoon, B.H., Kim, S.K., and Kim, S.Y. (2019). GENT2: an updated gene expression database for normal and tumor tissues. BMC Med. Genomics *12* (*Suppl 5*), 101.

Paterson, E.K., and Courtneidge, S.A. (2018). Invadosomes are coming: new insights into function and disease relevance. FEBS J. *285*, 8–27.

Peláez, R., Morales, X., Salvo, E., Garasa, S., Ortiz de Solórzano, C., Martínez, A., Larrayoz, I.M., and Rouzaut, A. (2017). β3 integrin expression is required for invadopodia-mediated ECM degradation in lung carcinoma cells. PLoS ONE *12*, e0181579.

Peláez, R., Pariente, A., Pérez-Sala, Á., and Larrayoz, I.M. (2019). Integrins: moonlighting proteins in invadosome formation. Cancers (Basel) *11*, 615.

Peterson, Y.K., and Luttrell, L.M. (2017). The diverse roles of arrestin scaffolds in G protein-coupled receptor signaling. Pharmacol. Rev. *69*, 256–297.

Petropoulos, C., Oddou, C., Emadali, A., Hiriart-Bryant, E., Boyault, C., Faurobert, E., Vande Pol, S., Kim-Kaneyama, J.R., Kraut, A., Coute, Y., et al. (2016). Roles of paxillin family members in adhesion and ECM degradation coupling at invadosomes. J. Cell Biol. *213*, 585–599.

Purayil, H.T., and Daaka, Y. (2018). β-Arrestin1 mediates hMENA expression and ovarian cancer metastasis. Proc. Natl. Acad. Sci. USA *115*, 2856–2858.

Revach, O.Y., and Geiger, B. (2014). The interplay between the proteolytic, invasive, and adhesive domains of invadopodia and their roles in cancer invasion. Cell Adhes. Migr. *8*, 215–225.

Rhodes, D.R., Kalyana-Sundaram, S., Mahavisno, V., Varambally, R., Yu, J., Briggs, B.B., Barrette, T.R., Anstet, M.J., Kincead-Beal, C., Kulkarni, P., et al. (2007). Oncomine 3.0: genes, pathways, and networks in a collection of 18,000 cancer gene expression profiles. Neoplasia *9*, 166–180.

Rosanò, L., and Bagnato, A. (2019). New insights into the regulation of the actin cytoskeleton dynamics by GPCR/β-arrestin in cancer invasion and metastasis. Int. Rev. Cell Mol. Biol. *346*, 129–155.

Rosanò, L., Spinella, F., Di Castro, V., Nicotra, M.R., Dedhar, S., de Herreros, A.G., Natali, P.G., and Bagnato, A. (2005). Endothelin-1 promotes epithelial-to-mesenchymal transition in human ovarian cancer cells. Cancer Res. *65*, 11649–11657.

Rosanò, L., Spinella, F., Di Castro, V., Dedhar, S., Nicotra, M.R., Natali, P.G., and Bagnato, A. (2006). Integrin-linked kinase functions as a downstream mediator of endothelin-1 to promote invasive behavior in ovarian carcinoma. Mol. Cancer Ther. *5*, 833–842.

Rosanò, L., Cianfrocca, R., Masi, S., Spinella, F., Di Castro, V., Biroccio, A., Salvati, E., Nicotra, M.R., Natali, P.G., and Bagnato, A. (2009). Beta-arrestin links endothelin A receptor to beta-catenin signaling to induce ovarian cancer cell invasion and metastasis. Proc. Natl. Acad. Sci. USA *106*, 2806–2811.

Rosanò, L., Cianfrocca, R., Spinella, F., Di Castro, V., Nicotra, M.R., Lucidi, A., Ferrandina, G., Natali, P.G., and Bagnato, A. (2011). Acquisition of chemoresistance and EMT phenotype is linked with activation of the endothelin A receptor pathway in ovarian carcinoma cells. Clin. Cancer Res. *17*, 2350–2360.

Rosanò, L., Spinella, F., and Bagnato, A. (2013a). Endothelin 1 in cancer: biological implications and therapeutic opportunities. Nat. Rev. Cancer *13*, 637–651.

Rosanò, L., Cianfrocca, R., Tocci, P., Spinella, F., Di Castro, V., Spadaro, F., Salvati, E., Biroccio, A.M., Natali, P.G., and Bagnato, A. (2013b). β-arrestin-1 is a nuclear transcriptional regulator of endothelin-1-induced β-catenin signaling. Oncogene *32*, 5066–5077.

Rosanò, L., Cianfrocca, R., Tocci, P., Spinella, F., Di Castro, V., Caprara, V., Semprucci, E., Ferrandina, G., Natali, P.G., and Bagnato, A. (2014). Endothelin A receptor/β-arrestin signaling to the Wnt pathway renders ovarian cancer cells resistant to chemotherapy. Cancer Res. *74*, 7453–7464.

Rosenberg, B.J., Gil-Henn, H., Mader, C.C., Halo, T., Yin, T., Condeelis, J., Machida, K., Wu, Y.I., and Koleske, A.J. (2017). Phosphorylated cortactin recruits Vav2 guanine nucleotide exchange factor to activate Rac3 and promote invadopodial function in invasive breast cancer cells. Mol. Biol. Cell *28*, 1347–1360.

Sakurai-Yageta, M., Recchi, C., Le Dez, G., Sibarita, J.B., Daviet, L., Camonis, J., D'Souza-Schorey, C., and Chavrier, P. (2008). The interaction of IQGAP1 with the exocyst complex is required for tumor cell invasion downstream of Cdc42 and RhoA. J. Cell Biol. *181*, 985–998.

Salani, D., Di Castro, V., Nicotra, M.R., Rosanò, L., Tecce, R., Venuti, A., Natali, P.G., and Bagnato, A. (2000). Role of endothelin-1 in neovascularization of ovarian carcinoma. Am. J. Pathol. *157*, 1537–1547.

Semprucci, E., Tocci, P., Cianfrocca, R., Sestito, R., Caprara, V., Veglione, M., Castro, V.D., Spadaro, F., Ferrandina, G., Bagnato, A., and Rosanò, L. (2016). Endothelin A receptor drives invadopodia function and cell motility through the β-arrestin/PDZ-RhoGEF pathway in ovarian carcinoma. Oncogene *35*, 3432–3442.

Smith, J.S., and Rajagopal, S. (2016). The β-Arrestins: multifunctional regulators of G protein-coupled receptors. J. Biol. Chem. *291*, 8969–8977.

Takkunen, M., Hukkanen, M., Liljeström, M., Grenman, R., and Virtanen, I. (2010). Podosome-like structures of non-invasive carcinoma cells are replaced in epithelial-mesenchymal transition by actin comet-embedded invadopodia. J. Cell. Mol. Med. *14* (*6B*), 1569–1593.

Tang, Z., Kang, B., Li, C., Chen, T., and Zhang, Z. (2019). GEPIA2: an enhanced web server for large-scale expression profiling and interactive analysis. Nucleic Acids Res. *47* (*W1*), W556–W560.

Tocci, P., Cianfrocca, R., Di Castro, V., Rosanò, L., Sacconi, A., Donzelli, S., Bonfiglio, S., Bucci, G., Vizza, E., Ferrandina, G., et al. (2019). β-arrestin1/YAP/mutant p53 complexes orchestrate the endothelin A receptor signaling in high-grade serous ovarian cancer. Nat. Commun. *10*, 3196.

Ward, J.D., Ha, J.H., Jayaraman, M., and Dhanasekaran, D.N. (2015). LPA-mediated migration of ovarian cancer cells involves translocalization of Gαi2 to invadopodia and association with Src and β-pix. Cancer Lett. *356* (*2 Pt B*), 382–391.

Wickström, S.A., Lange, A., Hess, M.W., Polleux, J., Spatz, J.P., Krüger, M., Pfaller, K., Lambacher, A., Bloch, W., Mann, M., et al. (2010). Integrin-linked kinase controls microtubule dynamics required for plasma membrane targeting of caveolae. Dev. Cell *19*, 574–588.

Williams, K.C., Cepeda, M.A., Javed, S., Searle, K., Parkins, K.M., Makela, A.V., Hamilton, A.M., Soukhtehzari, S., Kim, Y., Tuck, A.B., et al. (2019). Invadopodia are chemosensing protrusions that guide cancer cell extravasation to promote brain tropism in metastasis. Oncogene *38*, 3598–3615.

Wolf, K., Wu, Y.I., Liu, Y., Geiger, J., Tam, E., Overall, C., Stack, M.S., and Friedl, P. (2007). Multi-step pericellular proteolysis controls the transition from individual to collective cancer cell invasion. Nat. Cell Biol. *9*, 893–904.

Yang, J., Kasberg, W.C., Celo, A., Liang, Z., Quispe, K., and Stack, M.S. (2017). Post-translational modification of the membrane type 1 matrix metalloproteinase (MT1-MMP) cytoplasmic tail impacts ovarian cancer multicellular aggregate dynamics. J. Biol. Chem. *292*, 13111–13121.

Yeung, T.L., Leung, C.S., Yip, K.P., Au Yeung, C.L., Wong, S.T., and Mok, S.C. (2015). Cellular and molecular processes in ovarian cancer metastasis. A Review in the Theme: Cell and Molecular Processes in Cancer Metastasis. Am. J. Physiol. Cell Physiol. *309*, C444–C456.

Zagryazhskaya-Masson, A., Monteiro, P., Macé, A.S., Castagnino, A., Ferrari, R., Infante, E., Duperray-Susini, A., Dingli, F., Lanyi, A., Loew, D., et al. (2020). Intersection of TKS5 and FGD1/CDC42 signaling cascades directs the formation of invadopodia. J. Cell Biol. *219*, e201910132.

CellPress
OPEN ACCESS

STAR★METHODS

KEY RESOURCES TABLE

REAGENT or RESOURCE	SOURCE	IDENTIFIER
Antibodies		
Rabbit polyclonal anti-ILK	Genetex	Cat#GTX10169; RRID:AB_1950586
Rabbit monoclonal anti-β-arrestin1	Abcam	Cat#32099; RRID:AB_722896
Rabbit polyclonal anti-β-arrestin1	LSBio	Cat#LSC156512
Rabbit polyclonal anti-βPix	Cell Signaling Technology	Cat#4515
Mouse monoclonal anti-βPix (H-3)	Santa Cruz Biotechnology	Cat#sc-393184
Rabbit polyclonal anti-phospho-PAK1 (Thr423)/PAK2(Thr402)	Cell Signaling Technology	Cat#2601
Rabbit polyclonal anti-PAK1	Cell Signaling Technology	Cat#2602
Rabbit monoclonal anti-Rac3	Abcam	Cat#ab129062; RRID:AB_11143779
Mouse monoclonal anti-αTubulin	Santa Cruz Biotechnology	Cat#sc-32293; RRID:AB_628412
Mouse monoclonal anti-AU5 tag	Abcam	Cat#ab24576; RRID:AB_448153
Mouse monoclonal anti-MMP14	Santa Cruz Biotechnology	Cat#sc-12366; RRID:AB_673759
Rabbit polyclonal anti-phospho-Cortactin (Tyr421)	Abcam	Cat#47768; RRID:AB_869231
Rabbit polyclonal anti-Cortactin (H222)	Cell Signaling Technology	Cat#3503; RRID:AB_2115160
Mouse monoclonal anti-Cortactin [4F11]	Abcam	Cat#ab33333; RRID:AB_731713
Rabbit monoclonal anti-phospho-Cofilin (Ser3)	Cell Signaling Technology	Cat#3313; RRID:AB_2080597
Rabbit monoclonal anti-Cofilin (D3F9) XP	Cell Signaling Technology	Cat#5175; RRID:AB_10622000
Mouse monoclonal β-arrestin2	Santa Cruz Biotechnology	Cat#sc-13140
Rabbit polyclonal anti-FLAG	Cell Signaling Technology	Cat#2638
Rabbit polyclonal anti-ET_AR	Thermo Fisher Scientific	Cat#PA3-065
Mouse monoclonal anti-Threonine	Immunological Sciences	Cat#MAB-80131
Mouse monoclonal anti-Tyrosine	Immunological Sciences	Cat#MAB-94223
Rabbit polyclonal anti-Paxillin	GeneTex	Cat#GTX125891
Bacterial and virus strains		
BL21(DE3) Chemically Competent *E. coli*	Thermo Fisher scientific	C600003
Chemicals, peptides, and recombinant proteins		
Fibronectin human foreskin	Sigma-Aldrich	Cat#F2518-5MG
Collagen Type I rat tail	BD biosciences	Cat#MA01730
Collagen type I From Bovine Skin, Fluorescein Conjugate	Invitrogen	Cat#D12060
BQ-788 sodium salt	Bachem	Cat#4058874
N-cis-2,6-Dimethylpiperidinocarbonyl-β-tBu-Ala-D-Trp(1-methoxycarbonyl)-D-Nle-OH		
Cultrex Basement Membrane Matrix	Trevigen	Cat#3432-001-01
Ilomastat	Millipore	Cat#GM6001
Ambrisentan	Sigma-Aldrich	Cat#SML2104
Critical commercial assays		
Rac Activation Assay Biochem Kit	Cytoskeleton	Cat#BK035
Cultrex 3D Spheroid Cell Invasion Assay	Trevigen	Cat#3500-096-K
Experimental models: cell lines		
Human cell lines: SKOV3	American Type Culture Collection (ATCC)	ATCC® HTB-77; RRID:CVCL_0532

(*Continued on next page*)

Continued

REAGENT or RESOURCE	SOURCE	IDENTIFIER
Human cell lines: OVCAR3	American Type Culture Collection (ATCC)	ATCC® HTB-161; RRID:CVCL_0465
Human cell lines: CAOV3	American Type Culture Collection (ATCC)	ATCC® HTB-75; RRID:CVCL_0201
Human primary mesothelial cell	Zen-Bio	Cat#MSO-1; Cat#DME-F
Experimental models: organisms/strains		
Mouse: NOD/SCID 4-5 weeks (female)	Charles River laboratories	N/A
Oligonucleotides		
Primers for ILK: Forward: 5′-GAGAGCGGGCAGAGAAGATG-3′ Reverse: 5′-GAGTGTTTGTTCAGGGTTCCATTT-3′	Eurofins Genomics	N/A
Primers for βPIX(*PIXB*): Forward: 5′-AGCTCGAGAGACACATGGAGGATT-3′ Reverse: 5′-TCTGCAGCTCAAGCTCTTTCCTCT-3′	Eurofins Genomics	N/A
Primers for Rac3 (*RAC3*): Forward: 5′-GACGACAAGGACACC-3′ Reverse: 5′-CCTCGTCAAACAGTC-3′	Eurofins Genomics	N/A
Primers for β-arr1(*ARRB1*): Forward: 5′-GAGCACGCTCTTACCCTTTCAC-3′ Reverse: 5′-TCTCTGGGGCATACTGAACC-3′	Invitrogen	Cat#824370
Primers for Cyclophilin A: Forward: 5′- TTCATCTGCACTGCCAAGAC-3′ Reverse: 5′-TCGAGTTGTCCACAGTCAGC-3′	Eurofins Genomics	N/A
siRNA targeting sequence: ILK: (13.2) 5′-AUGAUUGUGCCUAUCCUUGAGAAGA-3′ 3′-UGUACUAACACGGAUAGGAACUCUUCU-5′	IDT integrated DNA technologies	N/A
SiRNA targeting sequence: βPIX (*PIXB*): (13.1) 5′-GAAAGAUAUCUUCUACUCUUCCCAA-3′ 3′-UACUUUCUAUAGAAGAUGAGAAGGGUU-5′	IDT integrated DNA technologies	N/A
SiRNA targeting sequence: Rac3 (*RAC3*): (13.1) 5′-GACGUCUUUCUGAUCUGCUUCUCTC-3′ 3′-GACUGCAGAAAGACUAGACGAAGAGAG-5′	IDT integrated DNA technologies	N/A
SiRNA targeting sequence: MT1-MMP: (13.1), (13.2) and (13.3) 5′-GGCAACAUAAUGAAAUCACUUUCTG-3′ 3′-UACCGUUGUAUUACUUUAGUGAAAGAC-5′ 5′-GCCAUGAAGUCUUCACUUACUUCTA-3′ 3′-GUCGCUACUUCAGAAGUGAAUGAAGAU-5′ 5′-UGUGGCUAAAAGGAAUCUAAUCUTG-3′ 3′-AAAGACCGAUUUUCCUUAGAUUAGAAC-5′	IDT integrated DNA technologies	N/A
SiRNA targeting sequence: TKS5 (*SH3PXD2A*): (13.2) 5′-CAAGCACUGAACACCGUCAACCAGA-3′ 3′-AGGUUCGUGACUUGUGGCAGUUGGUCU-5′	IDT integrated DNA technologies	N/A
SiRNA targeting sequence: β-arr1(*ARRB1*) SMARTpool	Dharmacon	Cat#L-011971-00
SiRNA targeting sequence: ET_AR (*EDNRA*) SMARTpool	Dharmacon	Cat#L-005485-00

(*Continued on next page*)

Continued

REAGENT or RESOURCE	SOURCE	IDENTIFIER
Recombinant DNA		
pGEX-4 T1 β-arrestin1	Nobles et al., 2007	Addgene plasmid # 36918; http://addgene.org/36918; RRID:Addgene_36918
AU5-β-arrestin1 full-lengtht	Richard D Ye from University of Illinois, Chicago, IL, USA	N/A
pcDNA3-β-arr1-FLAG	Dr Robert Lefkowitz Howard Hughes Medical Institute, Duke University, Durham, NC, USA	N/A
EDNRA GFP-tagged	OriGene Technologies	Cat# RG205385
pcDNA3.1 ILK-WT	Upstate Biotechnology	N/A
dominant-negative Src DN c-Src K296R/Y528F	Upstate Biotechnology	N/A
Software and algorithms		
ImageJ		https://imagej.nih.gov/ij/
GraphPad Prism 8		https://www.graphpad.com/scientific-software/prism/
GENT2	Park et al., 2019	http://gent2.appex.kr.
Gene Expression Profiling Interactive analysis (GEPIA) database	Tang et al., 2019	http://gepia.cancer-pku.cn/
Oncomine database	Rhodes et al., 2007	https://www.oncomine.org/
Gene Expression Omnibus (GEO) database GEO2R		https://www.ncbi.nlm.nih.gov/geo/geo2r/
Other		
Resource website for graphical abstract creation	this paper	https://biorender.com/

RESOURCE AVAILABILITY

Lead contact

Further information and requests for resources and reagents should be directed to and will be fulfilled by the Lead Contact, Laura Rosanò (laura.rosano@uniroma1.it).

Materials availability

This study did not generate new unique reagents.

Data and code availability

This study did not generate/analyze datasets/code.

EXPERIMENTAL MODELS AND SUBJECT DETAILS

For cell lines, established human high-grade ovarian serous adenocarcinoma cell lines SKOV3, OVCAR3, CAOV3 were obtained from the American Type Culture Collection (LGC Standards, Teddington, UK). OVCAR3 cells were maintained in RPMI-1640 medium (Cat# 618700-010; GIBCO Thermo Fisher), SKOV3 in McCoy's 5A medium (Cat# 26600-023; GIBCO Thermo Fisher) and CAOV3 in Dulbecco's modified Eagle medium (Cat#21885-025; GIBCO Thermo Fisher).

Human primary mesothelial cells (Cat# DMES-F) were obtained from Zen-Bio, inc, USA and maintained in Mesothelial Cell Growth Medium (Cat#MSO-1; Zen-Bio). All media were supplemented with 10% fetal calf serum, 50 units/mL penicillin and 50 mg/mL streptomycin. Cells were incubated at 37° C in a humidified atmosphere with 5% CO_2. When appropriate, cells were incubated in serum-free media with ET-1 at 100 nmol/L for the indicated times. Ambrisentan or BQ788 were used at the concentration of 1 μmol/L for 30 min before the addition of ET-1. Ilomastat was used at the concentration of 25 μM. All cells were tested routinely for mycoplasma contamination.

For in vivo animal studies, the experimental protocols comply with the principles of (https://arriveguidelines.org) and were approved by the National Ethics Committee for Animal Experimentation of the Italian Ministry of Health (Authorization N° 1/2020-PR #365869604). The mice were housed in single cages with wood-derived bedding material in a specific pathogen-free facility

with a 12h light/dark cycle under controlled temperatures (20–22 °C). Mice were cared for under the Principles of Laboratory Animal Care (National Institutes of Health publ. no. 85–23, revised 1985) and with national laws, and received water and food *ad libitum*. 4–6 weeks of age female NOD/SCID mice (Charles River Laboratories, Milan, Italy) were used.

METHOD DETAILS

Antibody and chemical reagents

Antibodies used for WB were as follows: anti-ILK (Cat# GTX101691; Genetex), anti-β-arr1 (Cat# ab32099; Abcam), anti-βPIX (Cat# 4515; Cell Signaling), anti-Phospho-PAK1 (Thr423)/PAK2 (Thr402) (Cat# 2601; Cell Signaling), anti-PAK1 (Cat# 2602; Cell Signaling), anti-Rac3 (Cat# ab129062; Abcam), anti-Tubulin (Cat# sc-32,293; Santa Cruz), anti-AU5 (Cat# ab24576; Abcam), anti-MT1-MMP (Cat# sc-12366; Santa Cruz), anti-Cortactin (Cat# 3503; Cell Signaling), anti-phospho-Cortactin Tyr 421 (Cat# ab47768; Abcam), anti-Cofilin (Cat# 5175; Cell Signaling), anti-phospho-Cofilin (Ser3) (Cat# 3313; Cell Signaling), anti-β-arr2 (Cat# sc-13140; Santa Cruz) and DYDDDDK (FLAG) Tag (Cat# 2368S; Cell Signaling), Endothelin A receptor (Cat# PA3-065; Thermo Fisher), anti-phospho-Threonine (Cat# MAB-80131) and anti-phospho-Tyrosine (Cat# MAB-94223; Immunological Sciences). Antibodies used for IF and PLA were as follows: anti-Cortactin (Cat# ab33333; Abcam), anti-Paxillin (Cat# GTX125891; Genetex), anti-βPIX (Cat# sc-137221; Santa Cruz), anti-β-arr1 (Cat# LSC156512; LSBIO), anti-ILK (Cat# GTX101691; Genetex), horseradish peroxidase-conjugated goat anti-rabbit or anti-mouse Abs, Alexa Fluor-488 and 594 secondary antibody (Thermo Fisher).

Chemical reagents used were as follows: Alexa Fluor 488 (Cat# A1101; Thermo Fisher), Alexa Fluor 594 (Cat# A11037; Thermo Fisher), Alexa Fluor 633 phalloidin (Cat# A22284; Thermo Fisher), Alexa Fluor 594 phalloidin (Cat# A12381; Thermo Fisher), 4',6'-diamidino-2-phenykindole (DAPI) (Cat# 1331762; Bio-Rad Laboratories), Vectashield (Cat# H-1000; Vector Laboratories), QCM Gelatin Invadopodia Assay (RED) (Cat# ECM671; Millipore), Calcein blue AM (Cat# C1429; Thermo Fisher), PKH26 Red Fluorescent Cell Linker Kit for General Cell Membrane Labeling (Cat# PKH26GL-1KT, Sigma-Aldrich), PKH67 Green Fluorescent Cell Linker Kit for General Cell Membrane Labeling (Cat# PKH67GL-1KT, Sigma- Aldrich), ET-1 (Cat# E7764-1MG; Sigma-Aldrich), BQ788 (1 μM) (Peninsula Laboratories), Ambrisentan (Cat# SML2104; Sigma-Aldrich) also called (+) - (2S) - 2-[(4,6dimethylpyrimidin-2-yl) oxy]-3-methoxy-3,3-diphenylpropanoic acid, Ilomastat (Cat# GM6001; Millipore). Fibronectin human foreskin (Cat# F2518-5MG; Sigma-Aldrich), Collagen Type I rat tail (Cat# MA01730; BD biosciences), Collagen type I From Bovine Skin, Fluorescein Conjugate (Cat# D12060; Invitrogen).

RNA isolation and RT-PCR

Total RNA was extracted from cells using Trizol Reagent (Thermo Fisher), according to the manufacturer's instructions and 1 μg were used for retrotranscription (RT) using Euro Script M-MLV Reverse Transcriptase (Euroclone). cDNA was examined by semiquantitative polymerase chain reaction (PCR), conducted in the automated DNA Thermal Cycler GeneAmp PCR System 9700 (Applied Biosystem) using AmpliTaq DNA Polymerase (Applied Biosystem). The primers used were as follow:

ILK F: 5′-GAGAGCGGGCAGAGAAGATG-3′
ILK R: 5′-GAGTGTTTGTTCAGGGTTCCATTT-3′
βPIX (*PIXB*) F: 5′-AGCTCGAGAGACACATGGAGGATT-3′
βPIX (*PIXB*) R: 5′-TCTGCAGCTCAAGCTCTTTCCTCT-3′
Rac3 (*RAC3*) F: 5′-GACGACAAGGACACC-3′
Rac3 (*RAC3*) R: 5′-CCTCGTCAAACAGTC-3′
β-arr1 (*ARRB1*) F: 5′-GAGCACGCTCTTACCCTTTCAC-3′
β-arr1 (*ARRB1*)R: 5′-TCTCTGGGGCATACTGAACC-3′
CyclophilinA F: 5′- TTCATCTGCACTGCCAAGAC-3′
CyclophilinA R: 5′-TCGAGTTGTCCACAGTCAGC-3′

The PCR products were analyzed by electrophoresis on 1% agarose gel and visualized by using ChemiDoc Imaging System and ImageLab Software (Bio-Rad Laboratories).

Silencing and transient transfection

Silencing of β-arr1 (L-011971-00) and ET_AR (L-005485-00) for 72h was performed using ON-TARGET plus SMART pool siRNAs (Di Modugno et al., 2018) and siGENOME Control Pool Non-targeting was used as a negative control (SCR) (Dharmacon). For silencing of ILK, RAC3, βPIX, MT1-MMP and TKS5 three selected pre-designed and validated siRNAs for a single target gene each were tested for their knockdown efficiency (ILK: hs.Ri.ILK.13.1, hs.Ri.ILK.13.2, hs.Ri.ILK.13.3; RAC3: hs.Ri.RAC3.13.1, hs.Ri.RAC3.13.2, hs.Ri.RAC3.13.3; βPIX: hs.Ri.βPIX.13.1, hs.Ri.βPIX.13.2, hs.Ri.βPIX.13.3; MMP14: hs.Ri.MMP14.13.1, hs.Ri.MMP14.13.2, hs.Ri.MMP14.13.3; TKS5: hs.Ri.TKS5.13.1, hs.Ri.TKS5.13.2, hs.Ri.TKS5.13.3 (TriFECTa kit, IA, USA) (Figure S11). The TriFECTa kit from IDT contains three Dicer-substrate 27-mer RNA duplexes that are specific. Each TriFECTa kit contains silencer-negative control. In brief, 1×10^5 cells were seeded and cultured in 6-well plates until they reached 30%–50% confluence and transiently transfected for 48h, using Lipofectamine RNAiMAX (Cat# 13778; Invitrogen) reagent according to the manufacturer's instructions. After

silencing the cells were lysed to confirm efficient knockdown, total cell lysate was collected at the endpoint of each experiment and analyzed by western blotting. The best knockdown efficiency (75%–90%) was obtained employing hs.13.2 for ILK, hs.13.1 for Rac3, hs 13.1 for βPIX, hs 13.2 for TKS5 and a pool of the three siRNAs for MMP14 (Figure S11). For transient ectopic expression of the AU5-β-arr1 full-length plasmid, we used constructs tagged with an AU5 epitope at their carboxyl termini kindly provided by Professor Richard D Ye (Department of Pharmacology, College of Medicine, University of Illinois, Chicago, IL, USA). The dominant-negative Src (DN-Src) was purchased from Upstate Biotechnology. For rescue experiments, we used the pcDNA3-β-arr1-FLAG wild-type plasmid construct, a 'wobble' mutant construct encoding rat β-arr1 sequences resistant to small interfering RNA targeting kindly provided by Dr Robert Lefkowitz (Howard Hughes Medical Institute, Duke University, Durham, NC, USA) for the ectopic expression of β-arr1. For the ectopic expression of human endothelin receptor type A (EDNRA), we used a C-terminal EDNRA GFP-tagged plasmid containing transcript variant 1 (Endothelin A Receptor (EDNRA) (NM_001957) Human Tagged ORF Clone, Cat# RG205385; OriGene Technologies). TrueORFs do not contain any UTR sequences All these plasmids were transfected for 24h by using Lipofectamine 2000 (Cat#11668-027; Invitrogen). The cDNA constructs have been obtained from Upstate (ILK cDNA allelic pack): wild-type ILK (ILK-WT), and control plasmid.

Western blotting (WB) and Immunoprecipitation (IP)

For WB analysis, total cells were detached by scraping, collected by centrifugation, and lysed in RIPA buffer [50 mMTris·HCL (pH 7.5), 150 mm NaCl, 1% Nonidet P-40, 0.5% sodium deoxycholate (NaDoc), 0.1% SDS] and proteases and phosphatase inhibitors (Roche). Protein concentrations were determined using the DC Protein assay (Bio-Rad Laboratories). Cell lysates were resolved on MiniPROTEAN TGX gels and transferred to nitrocellulose membranes (Bio-Rad Laboratories), followed by WB using the primary antibodies. Primary antibodies were revealed using horseradish peroxidase-conjugated goat anti-rabbit or anti-mouse Abs (Bio-Rad Laboratories). For the immunoprecipitation (IP), precleared whole-cell lysates were incubated with specific Abs or the correspondent IgG control Ab (Thermo Fisher) and protein A and G Sepharose beads (GE Healthcare) at 4 °C overnight. For detection of co-immunoprecipitated β-arr1, HRP-conjugated protein A peroxidase (Thermo Fisher) was used as secondary Ab. Proteins were visualized by chemiluminescence (Clarity Western ECL Substrates, Bio-Rad Laboratories). Quantification analyses were performed by ImageJ (https://imagej.nih.gov/ij/), a Java based freeware, and reflects the relative amounts as a ratio of each protein band relative to the lane's loading control.

Immunofluorescence and confocal laser scanning microscopy (CLSM)

Cells cultured on coverslips were fixed with 4% paraformaldehyde for 10 min at room temperature, permeabilized with 0.2% Triton X-100 and blocked with 0.1 M glycine, 1% BSA and 0.1% Tween20 in PBS for 30 min at room temperature. Samples were incubated with primary Abs in 0,5% BSA in PBS overnight at 4°C, followed by incubation with secondary Abs conjugated with Alexa Fluor 488 (Cat# A11001; Thermo Fisher) and Alexa Fluor 594(Cat# A11037; Thermo Fisher) for 1h at room temperature. Actin cytoskeleton was visualized by using Alexa Fluor 633 phalloidin (Cat# A22284; Thermo Fisher). Nuclei were stained with 4',6'-diamidino-2phenykindole (DAPI) (Bio-Rad Laboratories). Coverslips were finally mounted with a Vectashield mounting medium for fluorescence (Vector Laboratories). CLSM observations were performed with a Zeiss LSM980 apparatus, using a 63x/1.40 NA oil objective and excitation spectral laser lines at 405, 488, 543, 594 and 639 nm. Image acquisition and processing were carried out using the Zeiss Confocal Software Zen 3.1 (Blue edition). Signals from different fluorescent probes were taken in sequential scan settings and co-localization were visualized in merge images. Several cells for each labeling condition were analyzed and representative results are shown. All colocalization analyses were carried out using the Coloc2 plugin of ImageJ software to calculate Pearson's correlation coefficients. This software estimates the degree of overlap between fluorescence signals obtained in two separate fluorescent channels. The Pearson's coefficients were calculated from multiple images (n = 5–15) from 3 independent experiments and then averaged and a standard deviation of the mean was calculated.

Proximity ligation assay (PLA)

Briefly, cells (3×10^4 cells) were cultured on slides in a 24-well plate and stimulated for 15 min, then fixed with 4% paraformaldehyde for 10 min at room temperature, washed in PBS and blocked at 37°C with Duolink Blocking Solution. After blocking, cells were incubated with the primary Abs overnight at 4°C. Cells were washed with the wash buffer A and then incubated with Probe Anti-Mouse PLUS (Cat# DUO92001) and Probe Anti-Rabbit MINUS (Cat# DUO92005; Sigma-Aldrich) for 1 h at 37°C. Coverslips were washed with buffer A and then incubated with a DNA ligase diluted in Ligation buffer for 30 min at 37°C. After washing, coverslips were incubated with a DNA polymerase diluted in Amplification buffer for 120 min at 37°C. Slides were then washed with buffer B and incubated for 10 min with 4,6-diamidino-2-phenylindole dihydrochloride (DAPI). Coverslips were finally mounted with a Vectashield mounting medium for fluorescence. Red PLA signals (excitation/emission 598/634 nm) were identified as fluorescent spots by using a Leica DMIRE2 microscope equipped with a Leica DFC 350FX camera and elaborated by a Leica FW4000 deconvolution software (Leica). Images were imported in merged tiff formats containing both signal and nuclei channels. For each experimental condition, 15 randomly selected non-overlapping vision fields were analyzed and used for quantification analysis.

Inverted 3D collagen invasion assay

200 μl of 2.0 mg/ml collagen-I was allowed to polymerize in Transwell inserts (8-μm pores, Corning) for 2 h at 37°C. Cells were seeded on top of the collagen gel in serum-free medium, and stimuli and/or inhibitors were added to the medium in the bottom chamber of the Transwell as chemoattractants. After 48 h of seeding, cells were fixed and stained with DAPI and visualized by confocal microscopy with serial optical sections captured at 10-μm intervals with a 10 × objective on a Nikon A1R+ confocal unit on a Nikon Eclipse Ti-2 inverted microscope, using a 60x/1.40 NA oil-immersion objective and laser lines at 405, 488, 563, and 640 nm. Image acquisition and processing were carried out using the NIS Elements C software suite ver. 5.1. The invasion was measured by dividing the sum of signal intensity of all slides beyond 20 μm (invading cells) by the sum of the intensity of all slides (total cells), as per Zagryazhskaya-Masson A. et al., 2020).

Quantification of pericellular collagenolysis

Cells treated with indicated siRNAs were trypsinized and resuspended (2.5×10^5 cells/ml) in 200 μl ice-cold 2.0 mg/ml Collagen type I From Bovine Skin, Fluorescein Conjugate (Cat# D12060; Invitrogen). The collagen solution was adjusted to pH 7.5 using 0.34 N NaOH, and HEPES was added to 25 μM final concentration. 40 μl of the cell suspension in collagen was added on a glass coverslip, and collagen polymerization was induced for 30 min by incubation at 37°C. Serum-free medium was then added, and cells embedded in not-cross-linked collagen were stimulated and incubated for 16 h at 37°C. After fixation for 30 min at 37°C in 4% PFA in PBS, samples were incubated with anti-Col1-3/4C antibodies for 2h at 4°C.

After extensive washes, samples were stained with Alexa Fluor 594 anti-rabbit IgG (Cat# A11037; Thermo Scientific) antibody and counterstained with DAPI. Image acquisition was performed using an A1R+ Nikon confocal microscope with a 60 × NA 1.40 oil immersion objective, using a 561 nm laser excitation and a high-sensitivity GaASP detector with a 595/50 nm bandpass filter. Quantification of collagen degradation was performed as described by (Zagryazhskaya-Masson et al., 2020). Briefly, data were collected as the mean intensity of pericellular Col1-3/4C signal from maximum intensity projection of 10 optical sections with 2 μm interval from confocal microscope z stacks (20 μm depth) using NIS Elements (Nikon) software.

Gelatin zymography

To detect MMP-9 and −2 secretion and activity, conditioned media of untreated or treated cells were collected and concentrated by using Spin-X UF concentrator columns (Cat# 431483; Corning). Samples were separated by 9% SDS/PAGE gels containing 1 mg/mL gelatin. The gels were washed for 30 min at 22°C in 2.5% Triton X-100 and then incubated in 50 mM Tris (pH 7.6), 1 mM ZnCl2, and 5 mM CaCl2 overnight at 37°C. After incubation gels were stained with 0.2% Coomassie Blue. Enzyme-digested regions were identified as white bands on a blue background.

Fluorescent gelatin degradation assay

Coverslips were inverted on 200 μL drop of QCM Gelatin Invadopodia Assay (RED) (Millipore) and heated to 37°C. Coverslips were fixed in 0.5% glutaraldehyde for 15 min at 4°C and, after washing with PBS, were quenched with 5 mg/ml sodium borohydride for 3 min at room temperature. Slides were sterilized with 70% ethanol and left in complete growth media for 1h before use. Cells were cultured on gelatin-coated coverslips in a 24-well plate and left to adhere. Cells were then incubated for 48h in different experimental conditions and finally fixed and stained for CLSM examinations. Fluorescence signals were analyzed by Zeiss LSM980 Microscope equipped with a 63x oil objective. 3D-reconstruction images of selected regions of interest (ROI) with evident matrix degradation spots were shown. For the area of degradation, thresholding and particle size analysis were performed using Fiji. Experiments were done in triplicates by imaging > 10 fields of view and > 5 cells in each sample.

GTPase pull-down assays

To monitor Rac3 activation was used Rac Activation Assay Biochem Kit (Cat# BK035; Cytoskeleton). Cells were lysed in lysis buffer (50 mMTris (pH7.5), 10mM $MgCl_2$, 0.5 M NaCl and 2% Igepal and proteases inhibitors) and 500 μg of cell extracts were incubated with PAK (p21-Activated protein Kinase) PDB (p21 Binding Domain) beads to pull down Rac3-GTP forms and samples were rotated at 4°C for 60 min. Beads were washed, and proteins were eluted in Laemmli Sample Buffer by heating to 95°C for 2 min. Rac3 was detected using specific Abs.

Recombinant protein purification and GST-pull down assay

The plasmid pGEX-4 T1 β-arrestin1 [a gift from Robert Lefkowitz (Addgene plasmid #36918)] was transformed by heat shock into *E. coli* BL21. Transformed cells were grown in LB medium, supplemented with 50 μg/ml Ampicillin, till an OD 600 of 0.6-0.7 and induced with 1 mM isopropyl-thiogalactoside (IPTG) for protein expression, at 25°C overnight. From the cell-pellet, recombinant protein was purified using the MagneGST Protein Purification System (Promega), according to the manufacturer's instructions.

For GST-pull down assay, 300 μg of cell lysate, 10 μg of GST-protein and GST-fusion probe were incubated together with 50 μl of Glutathione-Sepharose beads for 2h at 4°C with end-over-end mixing. The samples were centrifuged at 1300 RPM for 2 min and the beads washed 3 times with ice-cold GST lysis buffer (20 Mm Tris-Cl (pH = 8), 200 Mm NaCl, 1 Mm EDTA (pH = 8), 0,5% NP-40, proteases inhibitor (Roche). After washes proteins were eluted in Laemmli 2X by heating to 95° for 5 min. Complexes recovered from the beads were analyzed by WB and detection of GST- β-arr1 was performed using GST (cat# SC-138, Santa Cruz) Abs.

Cell adhesion to mesothelial monolayer

SKOV3 ($20x10^3$) or OVCAR-3 after trypsinization were labeled with PKH67 Green Fluorescent Cell Linker for 5 min or blue Calcein for 30 min, washed two times and added to a 96-well microplate coated with a monolayer of human primary mesothelial cells. Cells were incubated with serum-free medium alone or with ET-1 and/or AMB and after 30 min non-adherent cells were removed by washing three times with serum-free medium. Adherent cells were photographed by using Bio-Rad ZOE fluorescent cell imager (Bio-Rad Laboratories) and the results of the analysis of the individual photos are reported, normalized to control and shown as a fold of control. The experiment was performed in triplicates for all conditions described and repeated at least three times.

Transmesothelial migration assay

Human primary mesothelial cells were seeded ($1x10^5$) in 8.0 μm pore sized membranes (Cat# 662638; Greiner bio-one) coated with fibronectin (10 μg/ml) and left to form a monolayer for 48h at 37°C. SKOV3 ($20x10^3$) and OVCAR3 ($40x10^3$) cells, in different experimental conditions, were stained with PKH26 Fluorescent (Cat# MINI26-1KT; Sigma-Aldrich) for 5 min at 37°C, washed with complete medium, plated onto a mesothelial monolayer, and allowed to migrate for 12h. Serum-free medium alone or with ET-1 and/or AMB were added to the lower chamber. Transmigrated cells were photographed by using Bio-Rad ZOE fluorescent cell imager (Bio-Rad Laboratories) and the results of the analysis of the individual photos are reported, normalized to control and shown as a fold of control. The experiment was performed in triplicates for all conditions described and repeated at least three times.

Transwell invasion assay

The assays were carried out using an insert 8.0 μm pore sized membranes (Cat# 662638; Greiner bio-one) coated Matrigel Invasion. Cells (4×10^4) were stimulated with serum-free medium alone or with ET-1 and/or AMB, added to the lower chamber precoated with Cultrex Basement Membrane Matrix (Cat# 3432-001-01Trevigen). The cells were left to migrate for 12h at 37°C. Cells on the upper part of the membrane were scraped using a cotton swab, and the migrated cells were stained using Three-Step Stain Set (Cat#3300; Thermo Scientific). The experiment was performed in triplicates for all conditions described and repeated at least three times. From each transwell, several images were taken by using Bio-Rad ZOE fluorescent cell imager under a phase-contrast microscope, and four broad fields were considered for quantification.

3D invasion assay

3D invasion assay was performed using Cultrex 3-D Spheroid Cell Invasion Assay (Cultrex #3500-096-K) according to the manufacturer's instructions. SKOV3 cells spheroids were generated by plating 3000 cells for 48 h in 3D Culture Qualified 96 Well Plate. Then, spheroids were embedded into not-cross-linked collagen I-based invasion matrix. After 1 h at 37 °C, serum-free media with or without ET-1 and/or AMB was added to spheroids wells. Plates were incubated for 72h and all spheroids were photographed by using Bio-Rad ZOE fluorescent cell imager (Bio-Rad Laboratories). Quantification of invasion area was measured using ImageJ software (https://imagej.nih.gov/ij/). Captured images were converted to 8 bit, the threshold was set to capture the total structure and calculate the invasive area outside the spheroid core.

In vivo experiments

Mouse *in vivo* adhesion assays were performed in the following way: 2×10^6 viable SKOV3-Luc cells were injected into the peritoneal cavity of mice (n = 5 per group). 8 h later, mice were sacrificed. Peritoneum, omentum, and mesentery were excised and *ex vivo* analysis performed. After gentle washing with PBS to eliminate non-adherent cells, the luminescence of the adherent cell aggregates was read and recorded. For testing antitumor metastatic efficacy of ambrisentan, mice were injected intraperitoneally with 200 μL PBS containing 2×10^6 viable SKOV3-Luc cells, following the guidelines for animal experimentation. Two weeks after, animals were randomized into two different groups undergoing the following treatments for 5 weeks: (i) 200 μL Metocell (vehicle, CTR), (ii) 200 μL ambrisentan (10mg/kg, oral daily), both by oral gavage. The experiment was performed twice with 6 mice per treatment arm per experiment. Mice were observed 2 times per week and monitored for signs of distress (i.e., changes in appearance, respiration, activity, etc.) and weighed; mice showing signs of distress or losing greater than 15% body weight were euthanized. Tumor burden was assessed on days 17, 25, 32, and 39 after tumor cell injection by measuring light emission following intraperitoneal luciferin administration. Briefly, 10 min after administration of D-luciferin (75 mg/kg body weight, intraperitoneal; Perkin Elmer, Hopkinton, MA, USA), photon emission was acquired for 5 min and analyzed with a CCD camera (Xenogen IVIS Lumina System; Perkin Elmer). Total flux (photons/second) was determined for the entire abdominal cavity per mouse and normalized to the mean total flux of control-treated mice imaged on day 17. Upon experimental termination (day 39), mice were euthanized and the number of visible metastases were measured and carefully dissected, frozen and analyzed for WB analysis.

QUANTIFICATION AND STATISTICAL ANALYSIS

Bioinformatics analysis

Analysis of Rac3 in cancers and normal tissues was carried out using GENT2 (http://gent2.appex.kr/gent2/) platform (Park et al., 2019). From GENT2 we selected data from GPL570 platform comprising 110 Normal samples and 285 Serous ovarian cancer samples.

The expression levels of Rac3 in ovarian serous carcinoma compared with that in the normal tissues (peritoneum) were identified from Yoshihara Ovarian Statistics data deposited in Oncomine Oncomine database (Reported ID: A_23_P336408) (Rhodes et al., 2007). The default settings were used and the threshold parameters were as follows: P value = 1×10^{-4}, fold change: 2 and gene rank in the top 10%.

To analyze the levels of Rac3 mRNA expression in ovarian cancer compared with those in normal specimens we used the online database GEPIA2, an interactive web-based tool that includes normal and tumor samples from the Genotype-Tissue Expression (GTEx) projects and TCGA for analyzing RNA sequencing expression data (Tang et al., 2019). The significance test method was one-way ANOVA, using disease state (Tumor or Normal) as the variable for calculating differential expression.

The gene expression profiles of Rac3 (GSE14407) was downloaded from the Gene Expression Omnibus (GEO) database (https://www.ncbi.nlm.nih.gov/geo), a public functional genomics data repository. The annotation platform was GPL570: [HG-U133_Plus_2] Affymetrix Human Genome U133 Plus 2.0 Array platform. Comparison of normal ovarian surface epithelia (OSE) and ovarian cancer epithelial cells (CEPIs). CEPIs were isolated by laser capture microdissection from serous papillary ovarian adenocarcinomas (Bowen et al., 2009).

To analyze the correlation of combination of EDNRA (204464_s_at) and ILK (201234_at) mRNA expression to overall survival (OS) and progression-free survival (PFS) in ovarian cancer a cohort of serous ovarian cancer patients (all stages) from all dataset was interrogated using the Kaplan-Meier plotter web tool (http://kmplot.com/analysis/index.php?p=service&cancer=ovar) (Gyorffy et al., 2012). The ovarian cancer patients were followed up to 5 years. To determine the prognostic value, the samples were split into two groups according to the median expression of the mean signal of the genes. The mRNA expression above or below the median separates the cases into high expression and low expression. Hazard ratio (HR), 95% confidence intervals, and log-rank P were presented on the main plots. P value of < 0.05 was considered to be statistically significant.

Statistical analysis

Statistical analysis was conducted using GraphPad Prism software and the values represent mean ± SD. Data were tested for normal distribution and Mann–Whitney nonparametric test was used when appropriated. Graphs comparing two conditions were analyzed via unpaired t test with Welch's correction. Graphs comparing more than two conditions were analyzed via one-way ANOVA followed by Tukey correction for multiple comparisons. Statistical significance was defined as *, $p < 0.05$; **, $p < 0.01$; ***, $p < 0.001$; ****, $p < 0.0001$. ns, not significant.